Pergamon

Prog. Solid St. Chem. Vol. 25, pp. 1–71, 1997
Published by Elsevier Science Ltd
Printed in Great Britain
0079-6786/97 $32.00

PII: S0079/6786(97)0003-4

MANGANESE OXIDES FOR LITHIUM BATTERIES

Michael M. Thackeray

Chemical Technology Division, Electrochemical Technology Program,
9700 South Cass Avenue, B-205 Argonne National Laboratory,
Argonne, Illinois 60439, U.S.A.

TABLE OF CONTENTS

ABSTRACT

Manganese oxides have been reviewed in the context of their application as host electrodes for rechargeable lithium batteries. The paper highlights the diversity of structure types found in the manganese oxide family, and how differences in structure affect the electrochemical profiles of Li/Li_xMnO_2 cells. The problems associated with the instability of manganese dioxides to lithium insertion and extraction which limits the performance of the cells, particularly cycle life, are discussed as are the methods that have been used to stabilize various MnO_2 structures.

1. INTRODUCTION

Manganese dioxide (MnO_2) has been exploited for many years as a battery grade electrode material. Although MnO_2 exists in many polymorphic forms, the gamma-form is historically known for its application in primary 1.5 V Zn/MnO_2 (aqueous) cells with electrolyte salts such as NH_4Cl (Leclanché cells), $ZnCl_2$ and KOH ("alkaline cells"). During the discharge of these cells, protons are inserted into the interstitial space of the gamma-MnO_2 structure; this process is accompanied by a simultaneous reduction of manganese ions by electrons introduced into the electrode by the external electrical circuit in order to maintain charge neutrality. The reaction at the positive H_xMnO_2 electrode is reversible up to a composition MnOOH (x = 1). Further discharge results in the irreversible formation of $Mn(OH)_2$. A rechargeable Zn/MnO_2 (alkaline) cell has recently been developed [1]. The cycle life is limited to approximately

25 cycles, largely because of morphological changes and gassing at the Zn electrode rather than by structural limitations at the positive MnO_2 electrode. The structural features and electrochemistry of MnO_2 electrodes in aqueous electrolytes have been comprehensively discussed in a recent review by Chabre and Pannetier [2].

The advent of electronic consumer products such as video cameras, laptop computers and cellular phones, and the need for lightweight batteries with high energy and power density has provided a major international drive to develop lithium batteries, and notably Li/MnO_2 batteries. Li/MnO_2 cells offer a significantly higher voltage than their Zn/MnO_2 analogues. The operating voltage of lithium cells depends not only on the manganese oxidation state, but also on the MnO_2 structure-type; it can vary between 5 V and 1 V. The use of metallic lithium as the negative electrode for rechargeable cells is unsafe because on repeated discharge and charge the lithium electrode becomes sponge-like, with extremely high surface area and reactivity with respect to organic liquid electrolytes. However, by using host structures for lithium, such as carbon (coke and graphite), lithium alloys, and metal oxides, several rechargeable lithium battery systems with manganese oxide positive electrodes have become a commercial reality. For example, over the last decade the following cells have appeared as commercial products: $Li_xC/Li_{1-x}Mn_2O_4$ (3.5 V lithium-ion cells); $LiAl/Li_xMnO_2$ (2.6 V coin cells); $Li_{4+x}Ti_5O_{12}/Li_{1-y}MnO_2$ (1.5 V coin cells). Recently, a new 3.5 V lithium-ion system that uses a glassy tin oxide negative electrode with a $Li_{1-x}Mn_2O_4$ (or $LiCoO_2$) positive electrode has been announced [3].

The large number of structure types that exists in the lithium-manganese-oxide system is attractive from the point of view that it offers a wide selection of materials [4]. On the other hand, the structural versatility of the system can make the processing of a desired single phase product with a specific composition difficult, particularly when scaling-up the process to the quantities required by the battery industry. This paper reviews the progress that has been made in developing new or modified lithium-manganese oxide electrode materials. The review stresses the current limitations of lithium-manganese-oxide materials and highlights the approaches that have been adopted in attempts to overcome these limitations. The relationship between structure and electrochemical properties is discussed and, particularly, how differences in structure affect the electrochemical profiles of Li/Li_xMnO_2 cells. The importance of maintaining structural integrity to achieve good cycle life is highlighted.

Several review papers on the structures and intercalation chemistry of transition metal oxides, often with a focus on lithium battery applications, have been published over the last two decades [5-12]. This review attempts to give an overall view of the complexity of the lithium-manganese oxide system and has been written particularly for those new to the field of lithium battery technology. Many figures have been used to illustrate the different structure-types, and the differences in their powder X-ray diffraction patterns and electrochemical behavior. (All X-ray diffraction patterns have been obtained with CuK_α radiation.) Most figures have been adapted from published data or taken directly from the literature. Because of the vast number of scientific papers on lithium-manganese oxides that have appeared in the literature over the past ten years, many of which are similar and confirm results already published, only a selected list of publications has been provided. Readers are encouraged to refer to these publications where more detailed information and additional references are available.

2. PROPERTIES OF INSERTION ELECTRODES FOR LITHIUM BATTERY APPLICATIONS

Lithium-ion cells operate by a mechanism whereby lithium ions shuttle between two host electrodes, commonly referred to as "insertion electrodes", during discharge and charge. The overall reaction that occurs in the cells can be represented as:

$$Li_xH' + H'' \rightleftharpoons Li_{x-y}H' + Li_yH'' \quad (1)$$

where H′ and H″ refer to the negative and positive electrodes, respectively. During discharge, y lithium ions are released from the negative electrode structure with a concomitant oxidation of the host H′ and inserted into the structure of the positive electrode H″, which is reduced. The reverse process occurs during charge. Ideally, lithium-ion cells should have the following properties:

- Reaction (1) should have a high large Gibbs energy ΔG, which provides a high cell voltage.

- There should be a limited variation in ΔG as the cell discharges (i.e. with increasing y) so that the operating voltage is as constant as possible.

- A fully-charged negative electrode, L_xH', should have a high oxidation potential, i.e. a low voltage with respect to metallic lithium, whereas a fully-charged positive electrode, H″, should have a low oxidation potential, i.e. a high voltage with respect to metallic lithium.

- The host structures should be as light as possible and should be able to accommodate a significant amount of lithium (i.e. a high y value) to provide high electrode capacities, generally expressed in mAh/g. (Cells with high voltage and electrode capacities will yield systems with high energy and power densities.)

- The lithium diffusion coefficient, D_{Li}, in the host electrodes should be as high as possible to provide cells with a high rate capability.

- The host electrodes should be good electronic conductors.

- The host electrodes should be stable over the entire voltage range and should be insoluble in, and should not react with, the electrolyte.

- The stability window of the electrolyte should be wider than the upper and lower operating voltage limits of the cell.

- There should be minimal modifications of the host electrode structures over the whole range of y, and minimal variation in the lattice parameters to ensure good reversibility.

- From a commercial and environmental standpoint, the materials should be inexpensive and non-toxic.

Over the years, many transition metal oxide materials have been investigated as insertion electrodes for lithium batteries, particularly the oxides of the first-row transition metal elements. The most important of these are the oxides of titanium, vanadium, manganese, iron, cobalt and nickel. The structural stability of these oxides to lithium insertion has recently been reviewed [13]. Most of these structures have close-packed oxygen arrays which are comprised of a network of oxygen tetrahedra and octahedra. In general, metal oxide structures with cubic-

close-packed (ccp) oxygen arrays are more stable to lithium insertion/extraction reactions than hexagonally-close-packed (hcp) arrays. In hcp structures, which have a packing sequence ABABAB , the octahedra share faces and edges with adjacent octahedra, whereas in ccp structures which have a packing sequence ABCABC , the octahedra share only edges with one another. The transition metal ions of the host electrode structure usually occupy octahedral sites. A hcp structure, therefore, shears toward ccp packing when lithium is inserted into the structure in response to electrostatic interactions between the lithium ions and the transition metal ions in face-shared octahedra.

Manganese oxide insertion electrodes have many of the properties that have been listed above. They are also inexpensive and non-toxic materials which make them attractive candidates as positive insertion electrodes. Manganese oxides can provide voltages up to 5 V vs. metallic lithium. The voltage of the cell depends not only of the formal valence state of the manganese ions, but also on the relative energy of the lithium sites in the various structures. Higher voltages are associated with increasing difficulty in removing a lithium ion from a particular site during charge; during discharge, the sites with the deepest energy wells will be occupied first. Most MnO_2 structures can accommodate one lithium per formula unit, i.e. until the rock salt stoichiometry $LiMnO_2$ is reached; the reaction involves the complete reduction of Mn^{4+} to Mn^{3+} and delivers an electrode capacity of 308 mAh/g. The reaction is analogous to the protonation of γ-MnO_2 electrodes to MnOOH during the discharge of Zn/MnO_2 cells [2].

Lithium insertion into MnO_2 materials is accompanied by modifications to the host structure; it can also cause irreversible structural damage. There are several main factors responsible for these structural modifications: (1) the instability of hexagonally-close-packed MnO_2 structures which shear on lithiation toward cubic close-packing, (2) the displacement of manganese ions into interstitial positions of the host structure, and (3) lattice distortions due to a Jahn-Teller effect when the concentration of Mn^{3+} (d^4) ions in the structure reaches a critical value (usually when the average manganese-ion oxidation state is approximately 3.5). The instability of MnO_2 structures to lithium insertion over a wide compositional range has, therefore, made it difficult to fabricate host electrode structures with high rechargeable electrochemical capacities. Despite these limitations, it has been demonstrated that it is possible to stabilize the structures of MnO_2 materials by selective substitution of manganese with other elements, or by reaction of MnO_2 with lithium oxide (Li_2O) to produce "lithia-stabilized" structures. These approaches have provided the motivation to continue the search for techniques

to improve the capacity and stability of state-of-the-art manganese oxide electrodes. In this regard, it should be noted that a practical rechargeable capacity of approximately 120 mAh/g can be obtained from $Li_x[Mn_2]O_4$ spinel electrodes at approximately 4 V against lithium [9]; this capacity corresponds to the insertion/extraction of 0.4 Li per Mn, or 81% of the theoretical value for the 4 V range ($0 \leq x \leq 1$). Taking into account only the masses of the active electrode materials and an average operating voltage of 4 V, this system offers an energy density of 480 Wh/kg. In practice, $Li_x[Mn_2]O_4$ spinel electrodes are of particular interest for "lithium-ion" cells that use lithiated-carbon electrodes Li_xC_6 ($x \leq 1$); these cells operate at a lower average voltage (3.5 V) and, by comparison, offer an energy density of approximately 300 Wh/kg. Other MnO_2 electrodes that operate at a lower average voltage (approximately 2.8 V vs. lithium), are of interest for lithium-polymer cells with metallic lithium negative electrodes; certain MnO_2 electrode structures have been shown to provide up to 250 mAh/g on the initial discharge (0.8 Li per Mn), but yield only 150-180 mAh/g on repeated charge and discharge [14]. With a rechargeable capacity of 160 mAh/g, these cells would, therefore, provide an energy density of 448 Wh/kg. A specific challenge that remains, therefore, is to develop stable 3 V MnO_2 structures (which are not as reactive to the cell environment as 4 V spinel-type materials), with superior rechargeable capacities to make them more competitive to 4 V systems. For example, a MnO_2 electrode with a rechargeable capacity of 200 mAh/g (0.65 Li per Mn), operating at an average 2.8 V in a metallic lithium/polymer-electrolyte cell would provide a cell with a relative energy density of 560 Wh/kg.

3. MnO_2 INSERTION ELECTRODES AND DERIVATIVE COMPOUNDS

3.1 Li-Mn-O Spinel Compounds

Lithium-manganese-oxide spinel electrodes are discussed first in this review because their structural and electrochemical properties provide much information about the behavior of other lithiated manganese oxide electrode systems. The early interest in spinel electrodes for lithium battery applications was spearheaded predominantly by the discovery that the $[B_2]X_4$ framework of many stable $A[B_2]X_4$ spinels, such as Fe_3O_4 [15], Mn_3O_4 [16,17] and $LiMn_2O_4$ [16-19] provided a stable host structure for the electrochemical insertion and extraction of lithium. During discharge of a lithium/spinel cell, the insertion reaction is accompanied by a simultaneous reduction of the A and/or B cations of the host. In general, spinel electrodes can

be lithiated to the rock salt stoichiometry ($LiA[B_2]X_4$) before the $[B_2]X_4$ framework is destroyed. The lithium spinels $Li[B_{2-x}Li_x]O_4$ (B= Mn [16-27], Ti [28-31], Co [32-34], V [35-38]; $0 \le x \le 0.33$) are of particular interest because the $[B_{2-x}Li_x]O_4$ spinel framework provides an uninterrupted and energetically accessible three-dimensional interstitial space of face-sharing tetrahedra and octahedra for Li^+-ion diffusion through the structure [19]. Moreover, it is possible to extract lithium from $Li[B_{2-x}Li_x]O_4$ structures with a concomitant oxidation of the B cations, thereby increasing the operating capacity of the spinel electrode over a wider compositional range.

3.1.1 The Li-Mn-O Phase Diagram. A representation of the Li-Mn-O phase diagram highlighting the positions of spinel and rock salt compositions within the λ-MnO_2, MnO and Li_2MnO_3 tie-triangle is shown in Fig. 1a; an expanded view of this tie-triangle is shown in Fig. 1b [25]. It shows the location of known structures and emphasizes the wide range of spinel and rock salt compositions that exist in the lithium-manganese-oxygen system. Stoichiometric spinels fall on the tie line between Mn_3O_4 and $Li_4Mn_5O_{12}$ (Fig. 1b), whereas stoichiometric rock salt compounds are located on the MnO- Li_2MnO_3 tie-line. Lithium insertion/extraction reactions into/from the spinel/rock salt phases are represented by dashed lines, which if extrapolated, converge at the Li apex of the phase diagram (Fig. 1a). The stoichiometric spinels of importance for lithium battery applications form a solid solution between $LiMn_2O_4$ and $Li_4Mn_5O_{12}$; they can be represented by the general formula $Li_{1+\delta}Mn_{2-\delta}O_4$ for $0 \le \delta \le 0.33$ [23, 25, 39, 40]. These spinels can be lithiated to their rock salt compositions which fall on the tie-line between $LiMnO_2$ and $Li_7Mn_5O_{12}$. Because lithium insertion into $Li_{1+\delta}Mn_{2-\delta}O_4$ spinels is accompanied by the immediate displacement of tetrahedrally-coordinated lithium ions into octahedral sites, the area that falls within the $LiMn_2O_4$ - $Li_4Mn_5O_{12}$ - $Li_7Mn_5O_{12}$ - $LiMnO_2$ quadrilateral represents a region of defect rock salt compositions. Extraction of lithium from the tetrahedral sites of $Li_{1+\delta}Mn_{2-\delta}O_4$ electrodes drives the composition of these spinels toward the MnO_2 - $Li_4Mn_5O_{12}$ tie line in the phase diagram; the area that falls within the MnO_2-$LiMn_2O_4$-$Li_4Mn_5O_{12}$ tie triangle, therefore, constitutes a region of defect spinel compositions. The various spinel structures that are of interest in the Li-Mn-O system can be defined by the three tie-lines of the MnO_2-$LiMn_2O_4$-$Li_4Mn_5O_{12}$ triangle. They represent the following systems: (i) $Li_x[Mn_2]O_4$ ($0 \le x \le 1$), (ii) $Li_{1+\delta}Mn_{2-\delta}O_4$ ($0 \le \delta \le 0.33$), and (iii) $Li_2O \cdot yMnO_2$ ($y \ge 2.5$). These three systems are discussed individually in the following sections.

a)

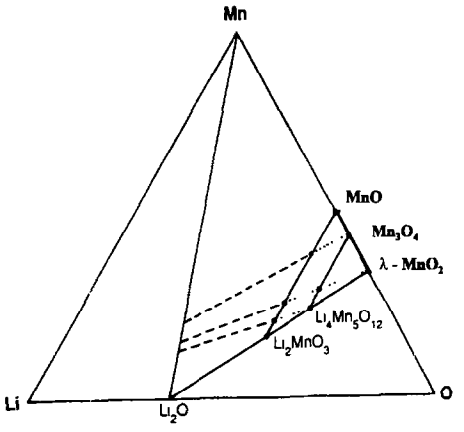

Fig. 1a

The Li-Mn-O phase diagram

(b)

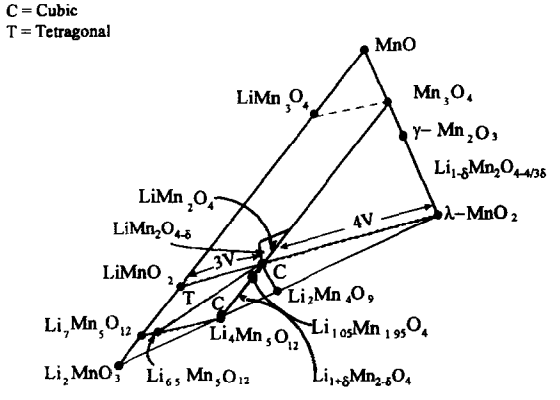

Fig. 1b

An expanded section of the phase diagram showing the compositions of spinel, defect spinel and rock salt structures [25, 81].

3.1.2 The System $Li_x[Mn_2]O_4$ ($0 \leq x \leq 2$). $Li[Mn_2]O_4$ is a cubic spinel with space group symmetry Fd3m. It can prepared by a simple solid state reaction of intimately mixed lithium and manganese oxide compounds, such as Li_2CO_3 and $MnCO_3$, in air at elevated temperature, typically 750°C [41]. The lithium ions are located on the 8a tetrahedral sites of the structure; the manganese ions are positioned on the 16d octahedral sites. The oxygen ions, which are cubic-close-packed (ccp) occupy the 32e positions. The structure of $Li[Mn_2]O_4$, showing the relative positions of Li, Mn and O is illustrated in Fig. 2a. The structure of the $[Mn_2]O_4$ spinel framework showing the octahedral coordination of the manganese ions and the three-dimensional interstitial pathways for lithium-ion diffusion is provided in Fig. 2b. It is important to note that in the spinel structure the MnO_6 octahedra are edge-shared and form a continuous three-dimensional cubic array (the manganese ions being distributed between alternate oxygen layers of the ccp array in a 3:1 ratio), thereby imparting a robustness and stability to the $[Mn_2]O_4$ spinel framework. Furthermore, of all the interstitial tetrahedra (8a, 8b and 48f) and octahedra (16c), the 8a tetrahedra are situated farthest from the 16d octahedra

occupied by manganese; they share each of their four faces with adjacent, vacant 16c octahedra. These structural features account for the unique stability of stoichiometric spinel compounds, many of which are found in nature, as exemplified by the stability of the prototype mineral, *spinel*, $Mg[Al_2]O_4$.

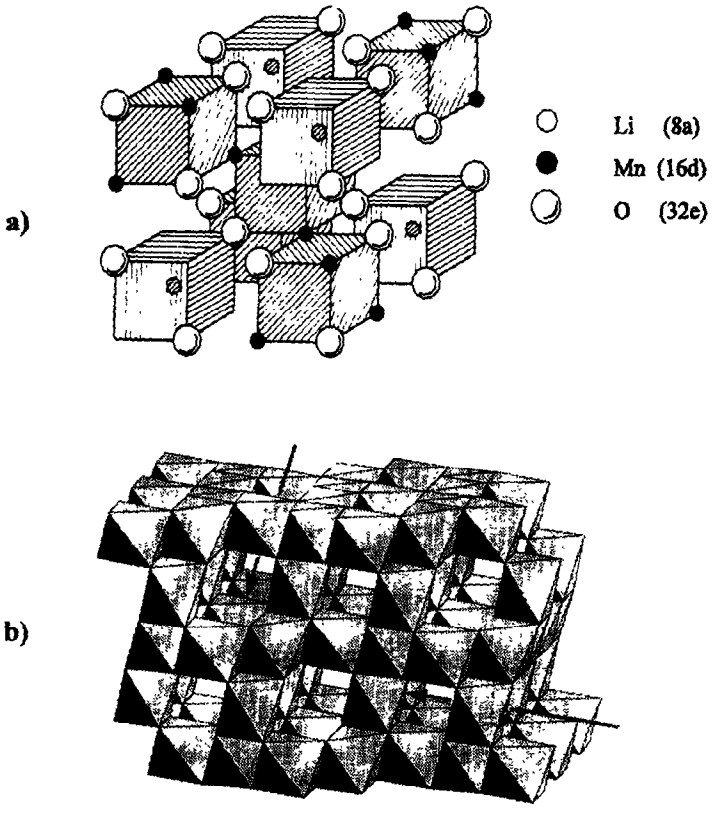

Fig. 2. Representations of (a) the structure of $Li[Mn_2]O_4$ [42], and (b) the $[Mn_2]O_4$ spinel framework [10].

A thorough evaluation of $Li_x[Mn_2]O_4$ spinel electrodes has been undertaken by numerous research laboratories [16-18, 20-22, 42-53]. The electrochemical profile of a $Li/Li_x[Mn_2]O_4$ cell for the range $0 \leq x \leq 2$ is shown in Fig. 3; the typical voltage response of the $Li_x[Mn_2]O_4$ electrode against a metallic lithium reference electrode is shown in a cyclic voltammogram in Fig. 4. The electrochemical data demonstrate that lithium is extracted from the tetrahedral sites of the spinel structure at approximately 4 V in a two-stage process, separated by only 150 mV [20] at a composition $Li_{0.5}[Mn_2]O_4$; The two-step process is due to ordering of the lithium ions on one-half of the tetrahedral 8a sites [17]. The high voltage associated with these two reactions can be attributed to the deep energy well in which the tetrahedral lithium ions reside, and the high activation energy, ΔE, that is required for the lithium ions to move from one 8a tetrahedron into

another 8a site via an energetically unfavorable neighboring 16c octahedron (see schematic illustration in Fig. 5a). The reason for the oxidation reaction at approximately 3.8 V that is sometimes observed during anodic scans of $Li[Mn_2]O_4$ spinel samples (Fig. 4) is not known.

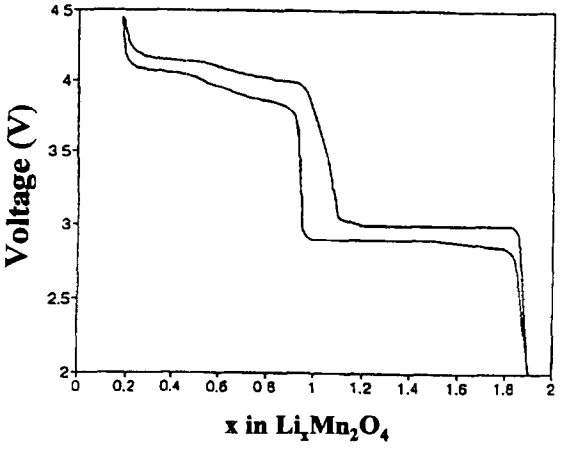

Fig. 3.

The electrochemical profile of a $Li/Li_x[Mn_2]O_4$ cell over the range $0<x<2$ [10].

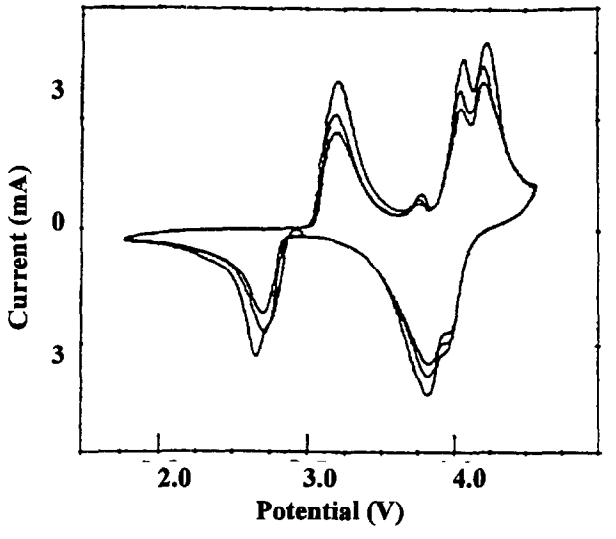

Fig. 4.

The cyclic voltammogram of a typical $Li[Mn_2]O_4$ electrode vs. a metallic lithium reference electrode [10].

Lithium insertion into $Li[Mn_2]O_4$ occurs at approximately 3 V (Fig. 3). During this process, lithium ions are inserted into the octahedral 16c sites of the spinel structure. Because the 16c octahedra share faces with the 8a tetrahedra, electrostatic interactions between the lithium ions on these two sets of sites cause an immediate displacement of the tetrahedral-site lithium ions into neighboring, vacant 16c octahedra. The reaction results in a first-order transition to $Li_2[Mn_2]O_4$ with a stoichiometric rock salt composition on the surface of the electrode particle. The electrochemical process at 3 V is thus a two-phase, constant voltage reaction. During discharge, a reaction front of $Li_2[Mn_2]O_4$ moves progressively from the surface

of the L i$[Mn_2]O_4$ particle into the bulk . In the rock salt phase, the octahedral 16c sites are of lower energy than the tetrahedral sites, as depicted schematically in Fig. 5b; in the rock salt structure, less energy is required to remove a lithium ion from the octahedral sites than from the tetrahedral sites of the$Li[Mn_2]O_4$ spinel phase. In fact, a structure analysis of a $Li_2[Mn_2]O_4$ sample with neutron data has indicated that the lithium ions may be distributed on both the 8a and 16c sites of the spinel structure (but predominantly on the 16c sites) [54], indicating that at this composition the difference in site energy between the octahedral and tetrahedral sites is relatively small. These results suggest that a lower activation energy (ΔE) for lithium-ion diffusion can be expected for the rock salt phase compared to the spinel phase.

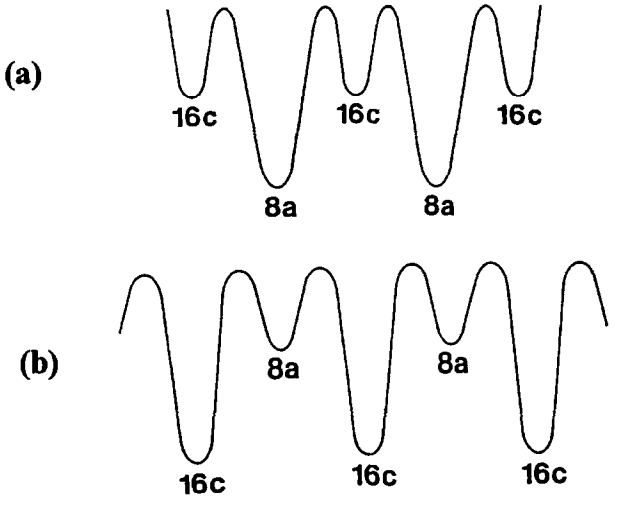

Fig. 5.

A schematic representation of the difference in site energies for the 8a tetrahedral sites and 16c octahedral sites (a) in the spinel $Li[Mn_2]O_4$, and (b) in the rock salt phase $Li_2[Mn_2]O_4$ [10].

The cubic symmetry of $Li_x[Mn_2]O_4$ electrodes is not affected by the electrochemical reaction at 4 V. Over the compositional range $0 \leq x \leq 1$, the lattice parameter varies from 8.245(1) Å in $Li[Mn_2]O_4$ to 8.029 Å in $[Mn_2]O_4$ (commonly referred to as λ-MnO_2 after Hunter) [55, 56]. Although the unit cell contracts and expands by 7.6 % over the 4 V range, it does so gradually and isotropically, which from a crystallographic standpoint, assists in combating structural degradation of the spinel electrode during cycling. In practice, however, capacity is lost slowly from $Li/Li_x[Mn_2]O_4$ cells when cycled between 4.2 V and 3.5 V (Fig. 6a). (Spinel electrodes that maintain cubic symmetry without any significant volume expansion/contraction during lithium insertion/extraction, such as $Li_4Ti_5O_{12}$, in spinel notation, $Li[Li_{0.33}Ti_{1.67}]O_4$, show excellent stability to electrochemical cycling [29-31].)

6a)

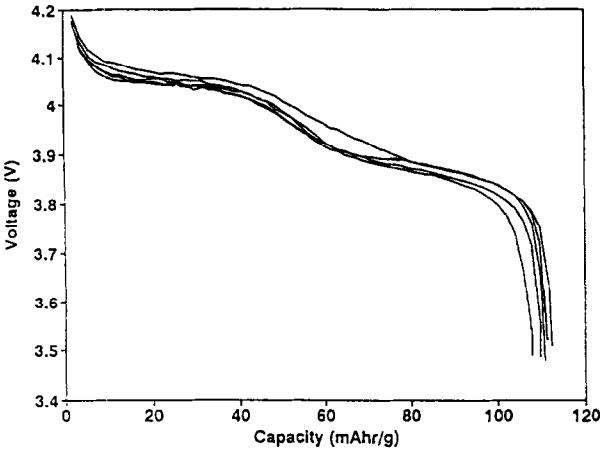

6b)

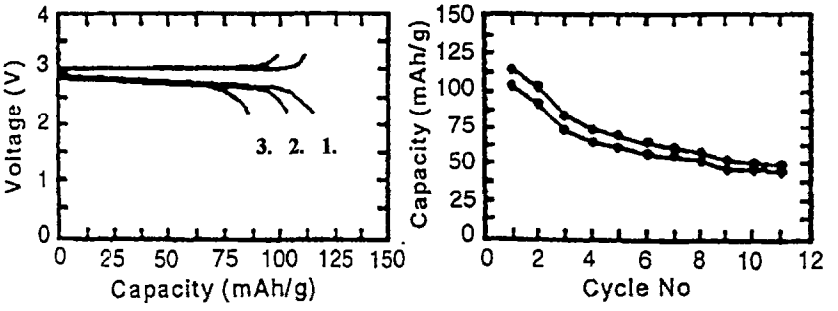

Fig. 6. Electrochemical cycling behavior of $Li/Li_x[Mn_2]O_4$ cells a) between 4.2 V and 3.5 V [10], and b) between 3.3 V and 2.2 V [23].

By contrast, lithium insertion into $Li_{1+x}[Mn_2]O_4$ electrodes at 3 V is accompanied by a severe crystallographic Jahn-Teller distortion as a result of an increased concentration of Mn^{3+} (d^4) ions in the $[Mn_2]O_4$ spinel framework, which reduces the crystal symmetry from cubic (c/a = 1.0) to tetragonal symmetry *(c/a* = 1.16) [16, 56]. The 16% increase in the *c/a* ratio is far too severe for the spinel electrode to withstand electrochemical cycling of lithium in and out of the structure. The strain imposed on the system is too great for the individual spinel particles to maintain structural integrity; they tend to break up and lose electrical contact, thereby resulting in rapid capacity loss of $Li/Li_x[Mn_2]O_4$ cells (Fig. 6b). The differences in crystallographic parameters of the $Li_x[Mn_2]O_4$ phases: λ-MnO_2 (x = 0), $Li[Mn_2]O_4$ (x = 1) and $Li_2[Mn_2]O_4$ (x = 2) are reflected in their powder X-ray diffraction patterns (Fig. 7a-c). The expansion of the unit cell that occurs on lithiating λ-MnO_2 (Fig. 7a) is reflected by the slight shift of the

diffraction peaks to smaller two-theta values in $LiMn_2O_4$ (Fig. 7b). Because lithium is a very weak scatterer of X-rays, the insignificant change in the relative intensities of the peak intensities reflects the structural stability of the $[Mn_2]O_4$ spinel framework. The extent of the tetragonal distortion (the *c/a* ratio) in $Li_2[Mn_2]O_4$ is reflected by the magnitude of the splitting of the peaks. For example, the [311] and [400] peaks of the cubic $Li[Mn_2]O_4$ phase (Fig. 7b) are split into the [113] and [311] peaks, and the [404] and [400] peaks of the tetragonal $Li_2[Mn_2]O_4$ phase, respectively (Fig. 7c).

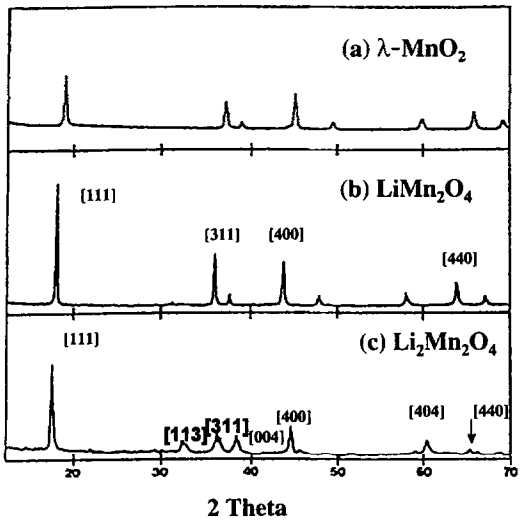

Fig. 7.

The powder X-ray diffraction patterns of a) λ-MnO_2, b) $Li[Mn_2]O_4$ and c) $Li_2[Mn_2]O_4$ [10].

The Jahn-Teller effect in lithium manganese oxide spinels has also been observed on lowering the temperature [57,58]. For example, cubic $Li[Mn_2]O_4$ undergoes a phase transition to tetragonal symmetry at 7 °C [57]; the extent of the tetragonal distortion is small (*c/a* = 1.011) compared to the distortion in $Li_2[Mn_2]O_4$ (*c/a* = 1.16) [16]. In the lithium-rich spinel phases $Li_{1+\delta}Mn_{2-\delta}O_4$ ($0<\delta\leq 0.33$), substitution of Mn by Li lowers the transition temperature significantly from to 7 °C to -59 °C [58].

3.1.3 Overdischarged $Li_xMn_2O_4$ Electrodes ($2\leq x\leq 4$). If $Li/Li_x[Mn_2]O_4$ cells are overdischarged, i.e. beyond a composition $Li_2[Mn_2]O_4$, open circuit voltage measurements have indicated a drop of voltage from 3 V to approximately 1.2 V (Fig. 8) [16]. Although the exact structures of overdischarged $Li_xMn_2O_4$ electrodes have yet to be characterized, it has been demonstrated that when $LiMn_2O_4$ is reacted chemically with an excess of n-butyllithium at 50°C, additional lithium can be incorporated into $Li_2[Mn_2]O_4$ to yield a layered structure $Li_4Mn_2O_4$

(Li_2MnO_2) [59]. This result, therefore, suggests that this is the reaction which occurs electrochemically at 1.2 V. Structure analysis of Li_2MnO_2 has shown that the oxygen array of $Li_2[Mn_2]O_4$ shears to hexagonal-close-packing in order to accommodate the extra lithium; the transformation to a layered structure necessitates the migration of 25% of the manganese ions from 16d sites in the lithium-rich layer into interstitial 16c sites in the manganese-rich layer of the spinel structure. In layered Li_2MnO_2, the octahedral sites of one layer and the tetrahedral sites of every alternate layer are fully occupied by Mn^{2+} and Li^+ ions, respectively (Fig. 9). Chemical treatment of Li_2MnO_2 with bromine has shown that the layered structure is unstable to delithiation and that it converts back to the spinel $Li[Mn_2]O_4$ [10, 60].

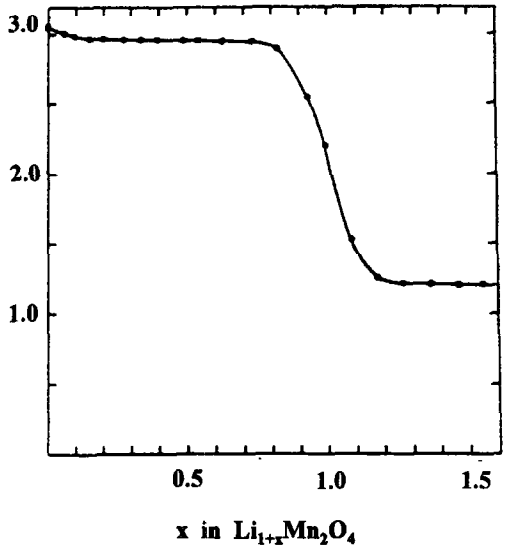

Fig. 8.

The open-circuit-voltage profile of a $Li/Li_{1+x}[Mn_2]O_4$ cell [16].

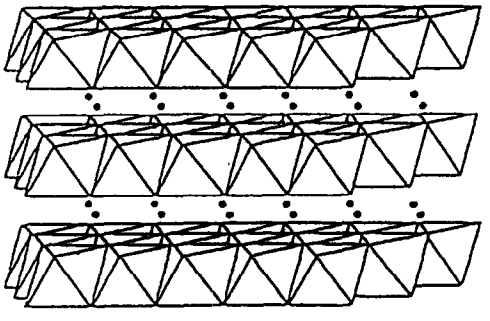

Fig. 9.

The layered structure of $Li_4Mn_2O_4$ (Li_2MnO_2). Mn^{2+} ions reside in the octahedra. o refer to Li^+ ions in tetrahedral sites [10].

3.1.4 $Li_{1+\delta}Mn_{2-\delta}O_4$ Electrodes ($0 \leq \delta \leq 0.33$). The slow capacity loss that has been observed in 4 V, liquid electrolyte, Li/Li$[Mn_2]O_4$ cells (Fig. 6a) has been attributed to several factors [25]:

(i) dissolution of manganese from the spinel electrodes, particularly if the electrolytes are slightly acidic. Dissolution can occur by a disproportionation reaction of extensively lithiated particles which contain a relatively high Mn^{3+} concentration:

$$2\ Mn^{3+}_{(solid)} \rightarrow Mn^{4+}_{(solid)} + Mn^{2+}_{(solution)} \qquad [2]$$

(ii) an instability of extensively delithiated spinel electrodes which are highly oxidizing in the cell environment, particularly with respect to organic electrolytes. This reaction, which can be accentuated by the presence of a carbon current collector in the positive electrode, can also lead to manganese dissolution [61].

(iii) the onset of a Jahn-Teller distortion at the end of discharge, when under dynamic conditions (thermodynamic non-equilibrium), the surface of the electrode particles are more extensively lithiated than they are in the bulk and can reach an overdischarged composition, in which the average oxidation state of the manganese ions is less than 3.5.

It is probable that all three factors given above may contribute to the capacity loss of 4 V $Li/Li_x[Mn_2]O_4$ cells. These factors can be at least partly circumvented by slightly modifying the composition of the spinel electrode by replacing a small fraction of the manganese ions in the $[Mn_2]O_4$ framework by lithium [25, 62]. These lithium-substituted spinel electrodes are represented by the general formula $Li_{1+\delta}Mn_{2-\delta}O_4$ ($0 \leq \delta \leq 0.33$); they are located on the tie-line between Li$[Mn_2]O_4$ and $Li_4Mn_5O_{12}$ in Fig. 1b.

For example, when δ=0.03, the spinel has the overall composition $Li_{1.03}Mn_{1.97}O_4$ in which the average manganese-ion oxidation state is increased from 3.50 in Li$[Mn_2]O_4$ to 3.54 [25]. The implication of this increased oxidation state is that the theoretical capacity of $Li_{1.03}Mn_{1.97}O_4$ electrodes at 4 V (136mAh/g) is lower than it is for Li$[Mn_2]O_4$ (148mAh/g) because only $0.91Li^+$ ions can be extracted from the structure before all the manganese ions reach the tetravalent state. Nevertheless, this disadvantage is compensated by the fact that lithium-substituted spinel electrodes combat all three factors given above. For example, increasing the

Mn^{4+} concentration in fully-discharged 4 V spinel electrodes will combat the dissolution of the electrode (point (i)) and the onset of the Jahn-Teller effect (point (iii)). Because the Jahn-Teller effect in Li-Mn-O spinel oxides is triggered, in general, when the average manganese oxidation state falls below 3.5, it is possible to insert a small amount of lithium into a cubic $Li_{1+\delta}Mn_{2-\delta}O_4$ phase at 3 V before the onset of the tetragonal distortion. In a $Li/Li_{1.03+x}Mn_{1.97}O_4$ (δ=0.03) electrode, the Jahn-Teller effect occurs when $x \approx 0.07$. Therefore, 4 V $Li_{1+\delta}Mn_{2-\delta}O_4$ electrodes have a safety "buffer" zone if they are slightly overdischarged. In fully-charged $Li_{1+\delta-x}Mn_{2-\delta}O_4$ electrodes, when $x \approx 0.91$ (e.g. $Li_{0.12}Mn_{1.97}O_4$ (δ=0.03)), there is always residual lithium which provides additional structural stability to the electrode (point (ii)); the end-of-charge is reached with an abrupt increase in voltage. These lithium-rich electrodes, therefore, have a built-in end-of-charge indicator.

The cycling behavior of a $Li/Li_{1.03-x}Mn_{1.97}O_4$ cell, operated over the 4 V regime is shown in Fig. 10. The discharge and charge profiles are similar to that of a standard $Li/Li[Mn_2]O_4$ cell (Fig. 6a), and are consistent with the insertion and extraction of the lithium ions into and from tetrahedral sites. Fig. 10 clearly illustrates the significant improvement in the capacity retention of lithium-rich spinels, such as $Li_{1.03}Mn_{1.97}O_4$ over the standard spinel $Li[Mn_2]O_4$ (Fig. 6a). The 0.03 Li^+ ions that occupy the 16d octahedra in $(Li)_{8a}[Mn_{1.97}Li_{0.03}]_{16d}O_4$ are locked in these sites and do not contribute to the capacity at 4 V because significantly higher voltage is required to dislodge them from their sites via energetically unfavorable face-shared 48f or 8b tetrahedra into the 16c-8a-16c-8a- diffusion pathways.

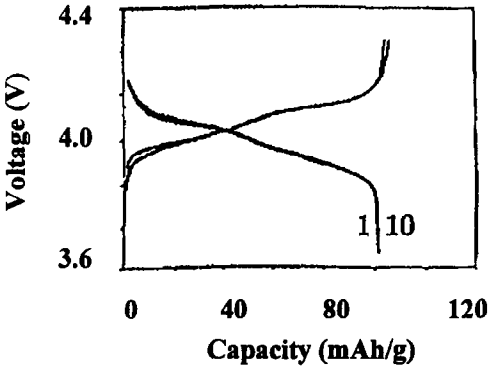

Fig. 10.

The cycling behavior of a $Li/Li_{1.03}Mn_{1.97}O_4$ cell [25].

The lithium-rich end-member of the $Li_{1+\delta}Mn_{2-\delta}O_4$ system is $Li_4Mn_5O_{12}$, or in spinel notation $Li[Mn_{1.67}Li_{0.33}]O_4$ (δ=0.33) [23, 39, 40, 63]. In this structure, which also has cubic

symmetry (Fd3m), the manganese ions are all tetravalent. It is, therefore, not possible to electrochemically extract any lithium from the structure, at least at practical voltages. Consequently, this electrode offers no capacity at 4 V. However, like $Li[Mn_2]O_4$, lithium can be inserted into $Li_4Mn_5O_{12}$ in a two-phase reaction at 3 V (Fig. 11). A major difference between $Li[Mn_2]O_4$ and $Li_4Mn_5O_{12}$ is that the Jahn-Teller distortion in $Li_{4+x}Mn_5O_{12}$ electrodes takes effect only late in the discharge when the average Mn oxidation state reaches 3.5, i.e. at a composition $Li_{6.5}Mn_5O_{12}$ ($x = 2.5$). For the range, $0 \leq x \leq 2.5$, the electrode maintains its cubic symmetry; the variation in the lattice parameter, a, is only 1%. The two-phases in the reaction are believed to be a cubic, lithiated spinel with a defect rock salt structure of composition $Li_{6.5}Mn_5O_{12}$ ($\{Li_{1.84}\square_{0.16}\}_{16c}[Mn_{1.67}Li_{0.33}]O_4$) on the particle surface and unreacted $Li_4Mn_5O_{12}$ within the bulk. This reaction renders $Li_{4+x}Mn_5O_{12}$ an attractive 3 V electrode for lithium battery applications, particularly if the composition of the electrode particles can be restricted to the cubic compositional range only. Lithiation beyond $x = 2.5$ results in the formation of tetragonal $Li_7Mn_5O_{12}$ with the stoichiometric rocksalt composition and an average manganese oxidation state of 3.4. It would be expected that the electrochemical formation of this phase would result in a two-phase reaction between $Li_{6.5}Mn_5O_{12}$ and $Li_7Mn_5O_{12}$. Surprisingly, no distinguishable voltage plateaus are observed during the early cycling of $Li/Li_4Mn_5O_{12}$ cells (Fig. 11). However, a point of inflection in the voltage profile has been observed to develop on the 3 V plateau on cycling these cells [60]. The tetragonal distortion in $Li_7Mn_5O_{12}$ (c/a=1.108) is not as severe as it is in $Li_2[Mn_2]O_4$, ($c/a = 1.16$) because of the lower concentration of Mn^{3+} ions in the former structure. These reactions with lithium-manganese-oxide spinel structures that occur at approximately 3 V are typical for Li_xMnO_2 compounds ($0 \leq x \leq 1$) in which lithium and manganese ions occupy octahedral sites in a close-packed oxygen array.

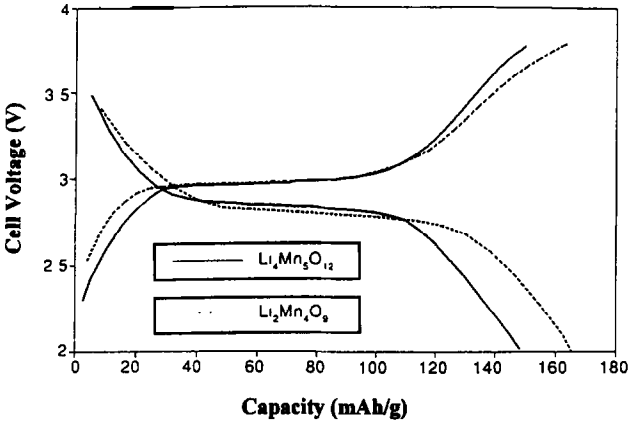

Fig. 11.

The initial discharge and charge profiles of $Li/Li_4Mn_5O_{12}$ and $Li/Li_2Mn_4O_9$ cells [4].

The principle of replacing some manganese ions by monovalent lithium to increase the mean oxidation state of the manganese ions to stabilize the spinel electrode structure (at 3 V or 4 V) can be extended to divalent or trivalent cations such as Mg^{2+} [25], Zn^{2+} [25], Co^{2+} [64-65], Ni^{2+} [65-68], or Cr^{3+} [65, 69-70]. For example, an electrode with composition $LiMg_{0.025}Mn_{1.975}O_4$ with an average manganese oxidation state of 3.52 shows enhanced capacity retention similar to that obtained from $Li_{1.03}Mn_{1.97}O_4$ electrodes [25]. In cases where stabilizing cations are used that can also partake in the electrochemical reactions, such as Co^{2+}, Ni^{2+} or Cr^{3+}, additional voltage plateaus are observed during the extraction of lithium. A good example is provided by the nickel-stabilized spinel $Li[Mn^{4+}_{1.5}Ni^{2+}_{0.5}]O_4$ [66]. This electrode contains sufficient Ni^{2+} to fully oxidize the remaining manganese ions in the spinel framework; it is, therefore, a similar electrode to $Li_4Mn_5O_{12}$ ($Li[Mn^{4+}_{1.67}Li^{+}_{0.33}]O_4$) and provides good cycling behavior at 3 V over the range $Li_{1+x}[Mn^{4+}_{1.5}Ni^{2+}_{0.5}]O_4$ ($0 \le x \le 1$). In this electrode, the Jahn-Teller effect is expected to occur late in the discharge, at a composition $Li_{1.75}[Mn^{4+}_{1.5}Ni^{2+}_{0.5}]O_4$ when the average oxidation state of the manganese ions reaches 3.5. Surprisingly, this distortion has not been observed in extensively lithiated samples [66]. However, unlike $Li_4Mn_5O_{12}$, lithium can be extracted from the tetrahedral 8a sites of $Li[Mn^{4+}_{1.5}Ni^{2+}_{0.5}]O_4$, because it is possible to oxidize the divalent nickel cations. This process, which occurs at 4.7 V, has been reported to involve the oxidation of Ni^{2+} directly to Ni^{4+} [67].

3.1.5 Lithia-Stabilized λ-MnO_2 (Spinel) Electrodes (Li_2O•yMnO_2, y≥2.5). Several compounds exist on the tie-line between λ-MnO_2 and Li_2O in the Li-Mn-O phase diagram (Fig. 1b); they can be represented by the general formula Li_2O•yMnO_2 [23, 71, 72]. These include the stoichiometric rock salt phase Li_2MnO_3 (y = 1) [73], the stoichiometric spinel phase $Li_4Mn_5O_{12}$ (y = 2.5), and what appears to be a solid solution of defect spinel phases for y>2.5, such as $Li_2Mn_3O_7$ (y = 3) [72], $Li_2Mn_4O_9$ (y = 4) [23, 71] and λ-MnO_2 (y = ∞) [55]. (Note that λ-MnO_2 may also be regarded as a defect rock salt phase, since the manganese cations partially occupy the octahedral sites and all the tetrahedral sites are vacant). The end members of the Li_2O•yMnO_2 system viz. λ-MnO_2 and $Li_4Mn_5O_{12}$ have already been discussed in sections 3.1.2 and 3.1.4. Of the intermediate compositions, $Li_2Mn_4O_9$ is the best characterized material; it has cubic symmetry, Fd3m, with a = 8.162 (X-ray data) [23, 71].

A neutron diffraction study of $Li_2Mn_4O_9$ has shown that the cation distribution in this defect spinel is $(Li_{0.89}\square_{0.11})_{8a}[Mn_{1.78}\square_{0.22}]_{16c}O_4$ [71]. Based on the arguments given in the preceding sections, it would be expected that lithium would be inserted first into the vacant

tetrahedral sites at 4 V, and thereafter into the 16c octahedral sites at 3 V. In practice, however, it has been demonstrated by both galvanostatic discharge of Li/ $Li_2Mn_4O_9$ cells and cyclic voltammetry studies of $Li_2Mn_4O_9$ electrodes that lithium is inserted on the initial discharge into the structure at 3 V (which implies octahedral occupation by lithium), but extracted on the subsequent charge at 3 V (removal from 16c octahedra) and 4 V (removal from 8a tetrahedra) (Figs. 12 and 13a [71]). The subsequent discharge in the cyclic voltammogram (Fig. 13a) shows that there is significant capacity at 4 V (peaks 5, 6) which is gained at the expense of capacity at 3 V (peak 7). If, however, the upper voltage limit for electrochemical cycling is restricted to 3.8 V, then excellent capacity retention is obtained at 3 V (Fig.13b). This behavior is not yet fully understood, although it may well be associated with the difficulties in synthesizing single-phase spinel compounds with predetermined compositions and well-ordered structures by solid state reactions at elevated temperatures (see section 3.1.6.). Note also that the voltage plateau of the Li/$Li_2Mn_4O_9$ cell at approximately 3 V in Fig. 11 extends almost to a composition $Li_4Mn_4O_9$ (142 mAh/g) when the mean oxidation state of the manganese ions reaches 3.5; this behavior is consistent with a two-phase electrode consisting of cubic $Li_2Mn_4O_9$ and cubic $Li_4Mn_4O_9$. It is expected that further lithiation would trigger the onset of the tetragonally-distorted $Li_5Mn_4O_9$ phase. Indeed, the powder X-ray diffraction pattern of a chemically-lithiated product with overall composition $Li_{3.7}Mn_4O_9$ can be indexed to a cubic unit cell (a = 8.171Å) [23]; the small change in unit cell volume (0.3 %) makes it difficult to distinguish the two cubic phases in the X-ray diffraction pattern. Further lithiation to a $Li_{4.4}Mn_4O_9$ clearly shows a two-phase product consisting, in this case, of a cubic phase of presumed composition $Li_4Mn_4O_9$ (a = 8.180Å) and a tetragonal phase of presumed rock salt composition $Li_5Mn_4O_9$ with lattice parameters a = 8.011Å and c = 9.150Å [23]. The mean oxidation state of the manganese ions in $Li_5Mn_4O_9$ is 3.25; the c/a ratio (1.14), has a value which is intermediate between that of $Li_2[Mn_2]O_4$ (c/a = 1.16) [16] and $Li_7Mn_5O_{12}$ (c/a = 1.11) [23].

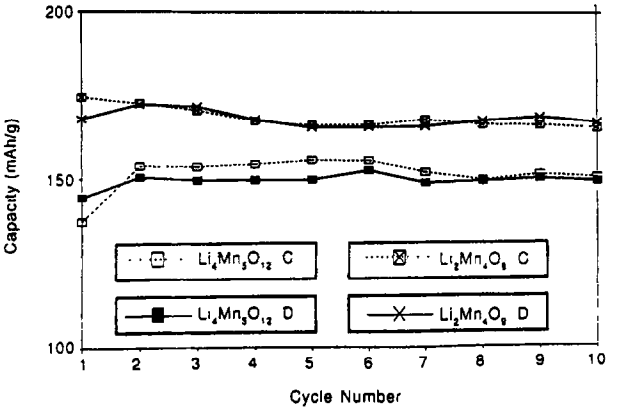

Fig. 12.

Capacity vs. cycling behavior for Li/$Li_4Mn_5O_{12}$ and Li/$Li_2Mn_4O_9$ cells. C = charge, D = discharge [4].

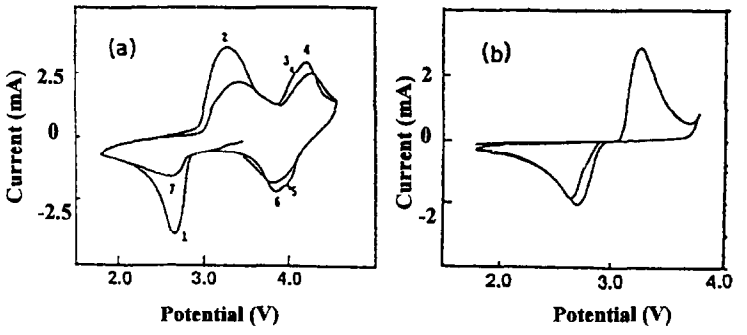

Fig. 13. The cyclic voltammograms of a $Li_2Mn_4O_9$ electrode vs. Li recorded (a) between 4.5 and 1.8 V and (b) between 3.8 and 1.8 V (scan rate = 1mV/s) [71].

3.1.6 The Thermal Stability of Lithium-Manganese-Oxide Spinels. The wide variety of lithium-manganese-oxide spinel compounds and the existence of large areas of solid solution makes it difficult to prepare single-phase compounds with predetermined compositions, particularly in large quantities. The control of processing parameters, particularly temperature to control the oxygen stoichiometry, and the need to use homogeneously mixed materials is, therefore, critically important in the fabrication of high quality materials. A great deal of effort has, therefore, been undertaken to devise reliable synthesis techniques and to understand reaction sequences and events that occur during processing [26, 74-90]. Nevertheless, the fact that numerous spinel compositions can be synthesized at moderate to high temperatures (300 - 800°C) reflects the stability of the $[Mn_{2-x}Li_x]O_4$ spinel framework and provides a good reason why many lithiated MnO_2 materials tend to transform to the spinel structure either, with the application of heat, or on electrochemical cycling.

The care that has to be taken in controlling temperature when preparing spinel compounds has been emphasized in studies of the thermal stability of $Li_{1+\delta}Mn_{2-\delta}O_4$ structures [26, 79, 81-83]. For example, it has been demonstrated by thermogravimetric analysis (TGA) and differential thermal analysis (DTA) and with high-temperature powder X-ray diffraction data recorded *in situ* when $Li[Mn_2]O_4$ is heated above 780°C (Figs. 14a and b) that the following reaction sequence occurs [81]:

a)

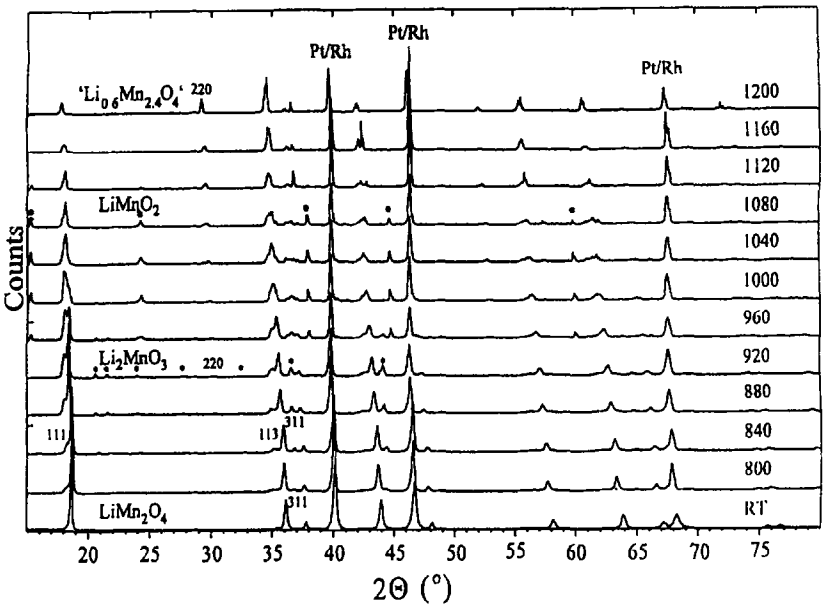

Fig. 14. a) The powder X-ray diffraction patterns of $Li[Mn_2]O_4$ recorded at room temperature (RT) to 1200°C. Peaks from Li_2MnO_3 (*) and $LiMnO_2$ (•) are indicated at 920 and 1080°C, respectively.

b)

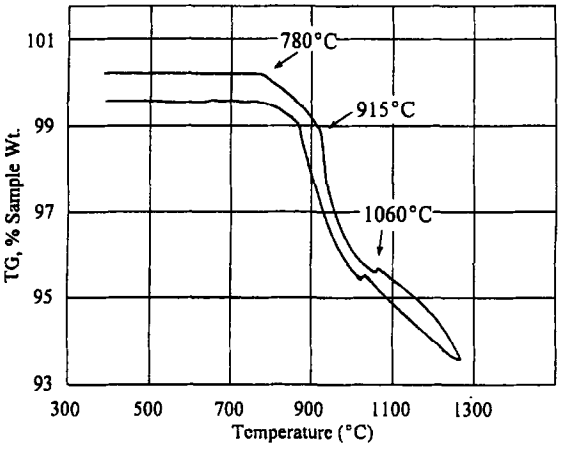

Fig. 14. b)

A TGA plot of $LiMn_2O_4$ [81].

1) At 780 - 915°C, oxygen is lost gradually from $Li[Mn_2]O_4$, which results in a disproportionation reaction of the stoichiometric spinel into a rock salt phase Li_2MnO_3 and an oxygen-deficient spinel phase $Li_{1-2\delta}Mn_{2-\delta}O_{4-2\delta-\delta'}$ with tetragonal symmetry (n^+_{Mn}<3.5, c/a = 1.02), according to the reaction:

$$Li[Mn_2]O_4 \rightarrow \delta\, Li_2MnO_3 + Li_{1-2\delta}Mn_{2-\delta}O_{4-2\delta-\delta'} + \delta'/2\, O_2 \qquad (3)$$

2) When the sample is heated above 915°C, oxygen is lost rapidly from the composite structure. A reduced rock salt phase $LiMnO_2$ (containing Mn^{3+}) forms at the expense of the Li_2MnO_3 rocksalt phase (containing Mn^{4+}) in the presence of the predominant $Li_{1-2\delta}Mn_{2-\delta}O_{4-2\delta-\delta}$, spinel phase. If it is assumed that no lithia is lost from the sample over this temperature range, then the reaction can be represented by a simplified reaction between a Li_2MnO_3 component and a predominant $Li[Mn_2]O_4$ component. For illustrative purposes only, the ideal stoichiometric reaction between the rock salt phase and the spinel phase for a 1:5 ratio would be:

$$Li_2MnO_3 + 5\ Li[Mn_2]O_4 \rightarrow 3\ LiMnO_2 + 4\ Li[Mn_2]O_4 + 1/2\ O_2 \qquad (4)$$

In this example, 20% of the spinel component is consumed by the Li_2MnO_3 phase to produce the $LiMnO_2$ phase. The $LiMnO_2$ phase is stable to approximately 1100°C.

3) At 1060°C, a phase transition of the tetragonal spinel phase to cubic symmetry occurs; this is similar to the transition of hausmannite, Mn_3O_4 from tetragonal to cubic symmetry which occurs at 1160°C [92]. At 1200°C, the product is a single-phase, cubic spinel which falls within the system $Li_{1-\delta}Mn_2O_{4-4/3\delta}$ ($0 \leq \delta \leq 1$). The overall reaction can, therefore, be represented:

$$Li[Mn_2]O_4 \rightarrow Li_{1-\delta}Mn_2O_{4-4/3\delta} + \delta/2\ Li_2O + 5\delta/12\ O_2 \qquad (5)$$

Rapid quenching of the 1200°C product to room temperature results in a tetragonal spinel phase with c/a = 1.12. Because the c/a ratio is a reflection of the concentration of Mn^{3+} on the octahedral 16d sites of the spinel framework, comparison of the c/a ratio with those of other spinel and rocksalt phases such as Mn_3O_4 (c/a = 1.16), $Li_2[Mn_2]O_4$ (c/a = 1.16), $Li_5Mn_4O_9$ (c/a = 1.14) and $Li_4Mn_5O_{12}$ (c/a = 1.11) implies that the quenched spinel phase has a composition $Li_{0.6}Mn_{0.4}[Mn_2]O_4$ and a structure in which Mn^{2+} ions are located on the tetrahedral sites as in Mn_3O_4 [81].

Overall, the reaction sequence may be viewed as one in which the composition of the initial spinel electrode is driven along the $Li[Mn_2]O_4$ - Mn_3O_4 tie line in the Li-Mn-O phase diagram [Fig. 1b]. As δ increases with increasing temperature, Mn^{2+} ions replace the Li^+ ions on the 8a tetrahedral sites of the spinel structure; at δ = 1, the limiting composition Mn_3O_4 is

reached. The exact temperature at which lithia starts to evaporate from the sample has not yet been unequivocally established; the TGA, DTA and XRD data suggest that it starts to occur during reaction 2 given above [81].

In general, the lithium-rich spinels $Li_{1+\delta}Mn_{2-\delta}O_4$ ($0<\delta\leq 0.33$) follow the same reaction sequence as that described for $Li[Mn_2]O_4$ above. However, because of the increased lithium content in these materials, the onset temperatures for the formation of the Li_2MnO_3 rocksalt phase is lower than it is for $Li[Mn_2]O_4$. For example, for $Li_4Mn_5O_{12}$ ($\delta=0.33$), the start of mass loss from the sample which is associated with the formation of Li_2MnO_3 has been detected by TGA analysis to be as low as 400 °C [82].

It has also been pointed out that in practice it is difficult to achieve fully-oxidized spinel products in the $Li_2O{\bullet}yMnO_2$ system, such as $Li_4Mn_5O_{12}$ (y = 2.5) and $Li_2Mn_4O_9$ (y = 4.0) by solid state reactions at high or moderately high temperatures; in most cases, these spinels are slightly oxygen-deficient and have an average manganese oxidation state between 3.9 and 4.0 [4, 23, 39, 93].

3.2 Thin-film $LiMn_2O_4$ Compounds Synthesized by Electron-Beam Evaporation or Radio-Frequency Magnetron Sputtering

3.2.1. Intergrown Spinel Structures?: The transformation to defect rock salt MnO_2. When the stoichiometric spinel $Li[Mn_2]O_4$ is used as a target material for the deposition of thin-film electrodes (approximately 0.5-1.0 μm thick) in solid state lithium cells by electron-beam evaporation or radio-frequency (r-f) magnetron sputtering, $LiMn_2O_4$ structures are formed that provide electrochemical characteristics that are significantly different to those provided by liquid electrolyte $Li/Li[Mn_2]O_4$ cells [94-95]. The solid state cells have the configuration $Li/lipon/LiMn_2O_4$, in which metallic lithium is used as the negative electrode and where lipon is an acronym for a glassy lithium-phosphorus-oxynitride solid electrolyte which is stable from 0 to 5.5 V vs. metallic lithium [96].

The electrochemical behavior of solid state $Li/lipon/LiMn_2O_4$ cells is compared to a typical Li/liquid electrolyte/$Li[Mn_2]O_4$ cell with a compacted powder $Li[Mn_2]O_4$ electrode in Fig. 15(a-d) [97-98]. Open circuit voltage measurements have shown that both types of cathode accommodate one lithium per Mn_2O_4 unit at 3 V. However, whereas lithium extraction from

$Li[Mn_2]O_4$ occurs in a two-step process near 4 V (Fig. 15a), the removal of lithium from electron-beam evaporated or r-f sputtered $LiMn_2O_4$ electrodes during an initial charge to 5.3 V takes place at 4 V, at 5 V and sometimes at 4.6 V (Figs 15(b-d)). The powder X-ray diffraction patterns of these electrodes indicate single-phase spinel-type products with lattice parameters slightly smaller than that of the standard spinel $Li[Mn_2]O_4$ (8.248 Å), typically $8.16Å \leq a \leq 8.20Å$ [95, 97]. The differences in electrochemical behavior of the electron-beam evaporated and sputtered $LiMn_2O_4$ electrodes can be attributed to differences in the distribution of the lithium and manganese ions within the cubic close packed oxygen array [97-98]. It has been proposed that this behavior can be accounted for by structures that can be regarded as an intergrowth of two spinel configurations, one defined by the conventional spinel notation $Li_{8a}[Mn_2]_{16d}O_4$ and the second by an alternative possible notation $Li_{8b}[Mn_2]_{16c}O_4$ [98] (see section 3.1.2 for crystallographic details of the spinel structure). An intergrown structure of two such spinels can, in principle, share a common cubic-close-packed oxygen lattice. Such a concept seems feasible since these thin-film electrodes are deposited atom by atom (or fragment by fragment) onto a platinum current collector. The presence of manganese ions on both sets of octahedral sites would necessarily destabilize the tetrahedral sites, thereby allowing the possible occupation of some 48f tetrahedral sites by lithium. Such an intergrown electrode would, therefore, have the configuration $\{Li_{1-x-y}\}_{8a,8b,48f}(Li_xMn_z\square_{2-x-z})_{16c}[Li_yMn_{2-z}\square_{z-y}]_{16d}O_4$ which represents a structure with both defect spinel and defect rock salt character. Although this configuration seems complex, it provides a fairly simple model to explain the electrochemical behavior of thin-film $LiMn_2O_4$ electrodes.

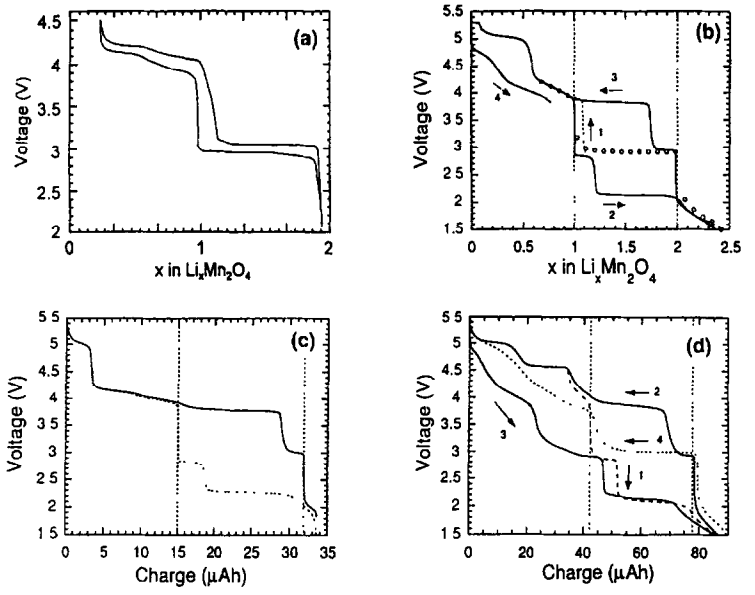

Fig. 15. Electrochemical charge/discharge profiles of (a) a standard liquid electrolyte Li/Li[Mn_2]O_4 cell (i = 0.2 mA), (b) three solid state Li/lipon/$LiMn_2O_4$ cells (i = 0.2 μA): (b,c) electron-beam prepared $LiMn_2O_4$, and (d) rf-sputtered $LiMn_2O_4$. Small circles in (b) are open-circuit voltage data. Numbers in (b) and (d) indicate the sequence of the charge/discharge processes [97, 98].

Despite the unusual distribution of cations in $\{Li_{1-x-y}\}_{8a,8b,48f}(Li_xMn_z\square_{2-x-z})_{16c}[Li_yMn_{2-z}\square_{z-y}]_{16d}O_4$, it is not unexpected that these electrodes discharge in a similar way to Li[Mn_2]O_4. Lithium insertion into the octahedral sites of both structure types will result in the displacement of tetrahedral lithium into neighboring vacant octahedral sites and at the same time lower the average manganese oxidation state below 3.5 to induce an immediate Jahn-Teller distortion, thus generating a constant voltage response at 3 V. By contrast, the electrochemical extraction of lithium from thin-film $LiMn_2O_4$ electrodes invokes an entirely different voltage response to standard Li[Mn_2]O_4 spinel electrodes (Fig. 15 (b-d)). Lithium extraction from thin-film $LiMn_2O_4$ electrodes between 3.8 and 4.5 V is associated with the removal of lithium from tetrahedral sites, whereas the relatively flat voltage plateaus at 4.6 V and 5.0 V that appear to be two-phase reactions have been attributed to the removal of lithium from the octahedral 16c and 16d sites, respectively. It has been proposed that the two-phase reaction at 4.6 V arises because of the disproportionation reaction [98]:

$$2\,Mn^{3+}{}_{16c,16d} \rightarrow Mn^{2+}{}_{8a} + Mn^{4+}{}_{16d} \qquad (6)$$

The suggested internal redox reaction generates a defect spinel phase in which Mn^{2+} (d^5) ions are stabilized in tetrahedral (8a) coordination (as in Mn_3O_4). Further extraction of lithium from the spinel phase necessitates the oxidation of the Mn^{2+} ions which immediately displaces these ions from their tetrahedral positions back to 16c octahedral sites because of the stronger preference of Mn^{3+} (d^4) and Mn^{4+} (d^3) ions for six fold coordination. This internal redox reaction (which may be dependent on localized concentrations (clusters) of manganese ions on 16c octahedral sites) results in a two-phase electrode with defect spinel and defect rock salt character. A similar reaction has been proposed for the extraction of lithium from the octahedral 16d sites at 5.0 V. The fully delithiated product is a defect rock salt phase MnO_2 with an unusual distribution of manganese ions on the 16c and 16d octahedral sites, $(Mn_z\square_{2-z})_{16c}[Mn_{2-z}\square_z]_{16d}O_4$. An important feature of this initial charge reaction to 5.3 V is that the distribution of manganese on the 16c and 16d sites in the fully delithiated product will not be the same as it is in the initial $LiMn_2O_4$ structure; rather, the manganese ions will tend to become randomly distributed over the 16c and 16d sites, because they can move through a common face from an 8a (8b) site into one of four 16c (16d) sites.

Of particular significance to the behavior of thin-film $LiMn_2O_4$ electrodes is that the two-phase reaction at 4.6 V on the initial charge does not appear on the subsequent discharge (Fig. 15d). This observation is consistent with the fact that it is most unlikely that a spinel-type phase with Mn^{2+} ions on tetrahedral sites would be regenerated during the early discharge of a defect rocksalt $Li_xMn_2O_4$ structure in which Mn^{4+} is reduced to Mn^{3+}. Furthermore, Fig. 15d shows that the initial discharge and subsequent charge of a $Li/Li_xMn_2O_4$ cell over the range $0 \le x \le 1$ are characterized by sloping voltage profiles between 5 V and 3 V. The shape of the profile, which indicates several reaction processes is dependent on the distribution of the manganese ions on the 16c and 16d sites of the defect rocksalt phase. If the manganese ions were randomly distributed over both sets of sites, there would be no clearly distinguishable pathways for lithium-ion diffusion through the structure. In such a situation, lithium extraction would be difficult, requiring high voltages, and the voltage profile of a $Li/Li_xMn_2O_4$ cell would be expected to have a single slope over the range $0 \le x \le 1$, characteristic of one single phase reaction process. This situation would be analogous to the formation of the rock salt ω-$Li_3V_2O_5$ structure [99] by electrochemical insertion of lithium into layered α-V_2O_5 [100]. In this case, vanadium ions diffuse into interstitial octahedra of $Li_xV_2O_5$ when $x>2$ to generate a robust rock salt structure in which the vanadium ions are almost randomly distributed over two-fifths of the octahedral sites in a close-packed oxygen array. Once formed, lithium is inserted into, and

extracted from, the ω-$Li_xV_2O_5$ structure in a single-phase reaction process between 1.5 and 4.0 V for the range 0<x<3 [99].

This electrochemical behavior of thin-film $LiMn_2O_4$ electrodes, produced by electron beam evaporation or pulsed laser-beam deposition, in liquid electrolyte lithium cells has not been evaluated above 4.5 V [101-103]. It is, therefore, not yet known whether the characteristics of these electrodes are similar to those of the thin-film electrodes in solid state Li/lipon/$LiMn_2O_4$ cells.

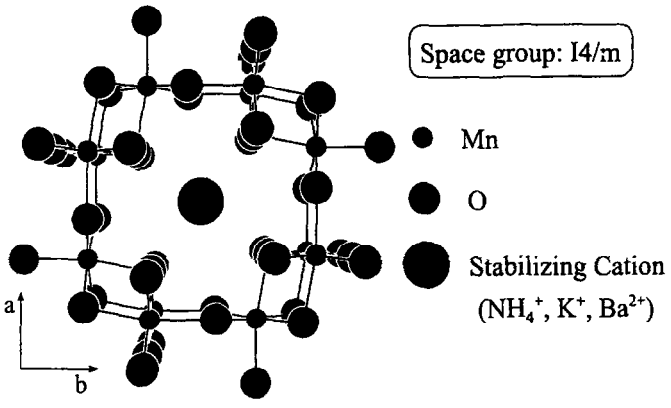

Fig. 16.

The structure of cation-stabilized α-MnO_2 [10].

3.3. Alpha-MnO_2

3.3.1 α-MnO_2 Electrodes. Alpha-MnO_2 exists in nature in several mineral forms such as hollandite ($BaMn_8O_{16}$) and cryptomelane (KMn_8O_{16}). The structures of these materials consist of interlinking double chains of MnO_6 octahedra and an interstitial space comprised of one-dimensional channels of relative dimensions (2 x 2) and (1 x 1) that extend in a direction parallel to the c axis of a tetragonal unit cell (Fig. 16). The Ba^{2+} and K^+ cations reside in the center of the (2 x 2) channels and provide stability to the structure. However, the presence of these large bulky cations impede the diffusion of lithium within the α-MnO_2 framework, thus limiting the application of these mineral forms of α-MnO_2 as insertion electrodes for lithium battery applications [104].

It has been demonstrated that the α-MnO_2 structure can be prepared in the absence of the large stabilizing cations, for example, by reaction of Mn_2O_3 or Li_2MnO_3 in concentrated sulfuric acid [105-107]. In these cases, the α-MnO_2 framework is stabilized by H_2O molecules

(or possibly H_3O^+ ions) that are located in the (2 x 2) channels. The water can be removed by heat treatment to 300°C without structural collapse (Fig. 17a). However, dehydrated α-MnO_2 products have a strong affinity for reabsorbing the water if exposed to air; if placed in water, the reaction can be quite violent. In this respect, α-$MnO_2 \cdot nH_2O$ materials behave in a similar way to zeolitic molecular sieves.

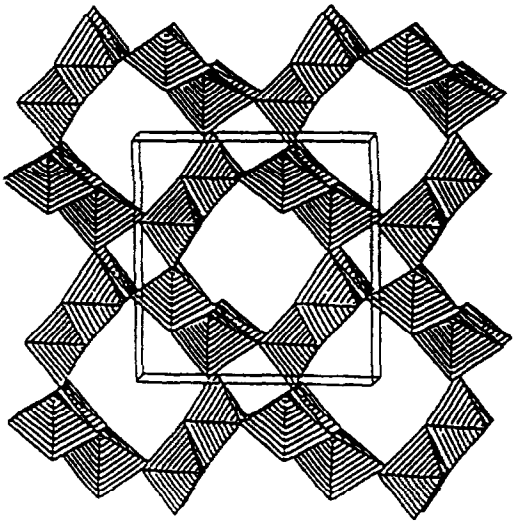

Fig. 17a.

The structure of anhydrous α-MnO_2 after heat treatment.

Electrochemical studies of anhydrous α-MnO_2 electrodes in non-aqueous lithium cells have shown that the α-MnO_2 framework can accommodate a significant amount of lithium on the initial discharge to 2.0 V, yielding a capacity in excess of 210 mAh/g (i.e., approximately 0.7 Li per Mn (Fig. 17b) [105]. However, electrochemical cycling over the voltage range 3.8 V to 2.0 V results in a sharp decrease in cell capacity [107]. This loss in capacity is believed to be associated with an instability of the (2 x 2) channels to electrochemical cycling, and that manganese and oxygen ions are displaced from the framework into the (2 x 2) channels to stabilize the structure. The diffusion of manganese into the (2x2) channels is significant because it would result in stabilized Li_xMnO_2 structures with defect rock salt character, similar perhaps to those created during the cycling of thin-film electrodes described in section 3.2. In such situations, it should be possible to regain the "lost capacity" of lithiated α-MnO_2 electrodes by charging cells to higher voltage.

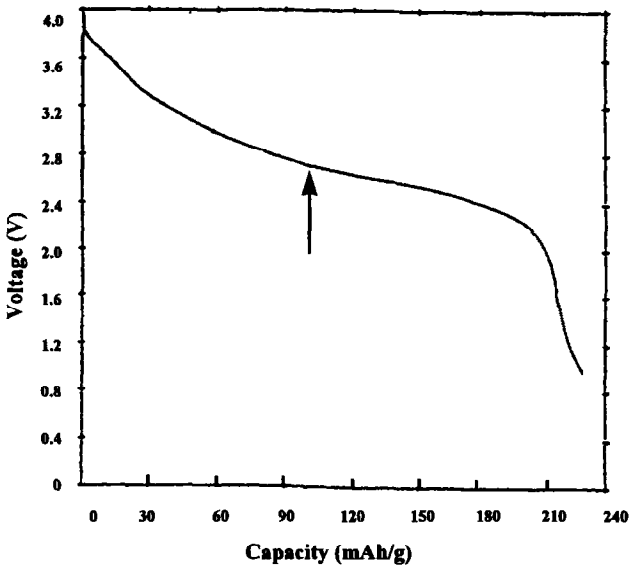

Fig. 17b.

The initial discharge of a Li/α-MnO_2 cell. The arrow indicates the onset of the second step of the reaction [105].

3.3.2 Lithia-Stabilized α-MnO_2 Electrodes. It has been demonstrated that enhanced performance and, particularly stability to electrochemical cycling can be achieved by reacting an ammonia-stabilized α-MnO_2 structure ($NH_4Mn_8O_{16}$) with LiOH at 300-400°C [108-110]. In this reaction, a lithiated α-MnO_2 product, "Li_xMnO_2" is obtained by ion-exchange. The precise structural features of the product are difficult to determine by X-ray and neutron diffraction techniques because the materials tend to be poorly crystalline and are contaminated with salts from the reaction process. However, the synthesis of highly crystalline α-MnO_2•nH_2O ($0.20 \leq n \leq 0.36$) products (from Mn_2O_3 and Li_2MnO_3 precursors) that can be lithiated with LiOH at 270°C without significant loss of crystallinity has made it possible to determine the structural features of lithium-stabilized α-MnO_2 products [107]. These reactions have shown that the α-MnO_2 framework can be stabilized by exchange of the H_2O component in α-MnO_2•nH_2O products with Li_2O, and that n can reach a value of 0.15 (in nLi O) without structural degradation of the α-MnO_2 framework. In practice, the manganese ions are not quite fully-oxidized; the products are slightly oxygen-deficient having an average manganese oxidation state between 3.9 and 4.0. Note that, if n = 0.25, the product transforms slowly on heating in air, even at 275°C, to an "oxygen-rich" spinel $LiMn_2O_{4+\delta}$ ($\delta \leq 0.5$), thereby endorsing the structural stability of lithium-manganese-oxide spinel compounds within selected compositional ranges (see section 3.1.6) [111].

Stabilization of the α-MnO_2 structure with lithia or reaction of α-MnO_2 with LiI does not alter the crystal symmetry, nor does it significantly change the lattice parameters of the

Table 1. Crystallographic parameters of α-MnO_2 materials [107].
(Space Group = I4/m)

Compound	*a* (Å)	*c* (Å)	Volume (Å^3)	Volume Expansion (%)
α-MnO_2 (anhydrous)	9.750 (1)	2.861 (1)	272.0	-
α-MnO_2•nH_2O (n≈0.3)	9.810 (1)	2.850 (1)	274.3	0.8
α-MnO_2•0.05Li_2O	9.818 (1)	2.859 (1)	275.6	1.3
α-MnO_2•0.10Li_2O	9.904 (1)	2.853 (1)	279.8	2.9
α-MnO_2•0.15Li_2O	9.965 (1)	2.850 (1)	283.0	4.0
α-MnO_2•0.20Li_2O	9.957 (1)	2.850 (1)	282.6	3.9
α-MnO_2•0.25Li_2O *	9.957 (1)	2.847 (1)	282.3	3.8

* two-phase product with some spinel

tetragonal unit cell as can be seen by the similarity of the X-ray diffraction patterns (Fig. 18(a-d)) [107], and the crystallographic parameters of α-MnO_2•nH_2O (n≈0.3), dehydrated α-MnO_2 , and lithia-stabilized nLi_2O•MnO_2 materials (Table 1). For $0.15Li_2O$•MnO_2, the *a* lattice parameter is marginally larger (2.2%) than it is in the anhydrous α-MnO_2 parent compound, the *a* lattice parameter is not significantly affected by lithiation, and the volume increase by 4%.

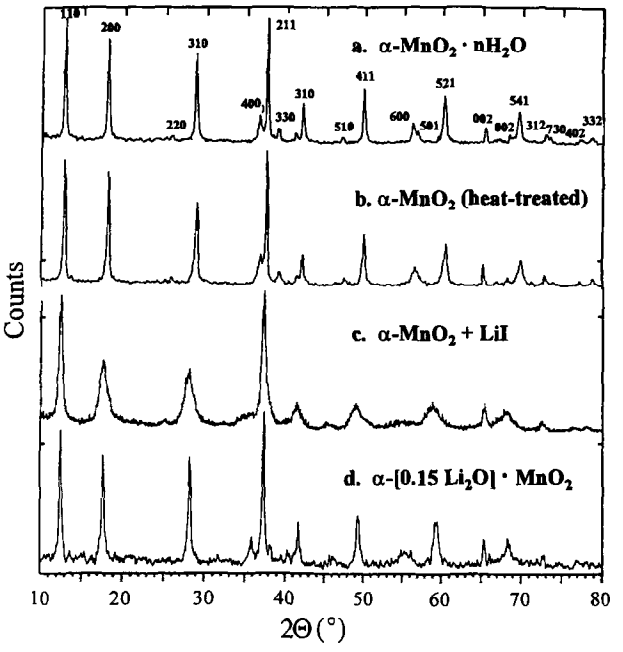

Fig. 18.

The powder X-ray diffraction patterns of
(a) α-MnO_2•nH_2O (n≈0.3),
(b) anhydrous α-MnO_2,
(c) after reaction with LiI, and
(d) lithia-stabilized $0.15Li_2O$•MnO_2 [107].

The lithia-stabilized α-MnO_2 structure (with the ideal, fully oxidized composition $0.15Li_2O$•MnO_2, or alternatively, $Li_{0.3}MnO_{2.15}$) is shown in Fig. 19. The oxygen ions of the Li_2O molecules are located at the same crystallographic sites in the (2 x 2) channels as the oxygen ions from H_2O in the water-stabilized product, α-MnO_2•nH_2O; these positions are close to those occupied by cations such as Ba^{2+}, K^+ and Na^+ in cation-stabilized α-MnO_2 structures. Of particular significance is that the oxygen ion from the Li_2O molecule partially occupies an anion vacancy in a defect (and slightly distorted) close-packed oxygen array, thus providing greater stability to the α-MnO_2 structure; it assists the prevention of a structural collapse of the (2 x 2) tunnels during the electrochemical cycling of lithium. The lithium ions in the $0.15Li_2O$•MnO_2 structure also reside in the (2 x 2) channels and are coordinated the oxygen ions of the framework and to the oxygen ion in the center of the channel (Fig. 19); in the structure analysis, no lithium could be detected in the narrow (1 x 1) channels [107]. Because the lithium ions in $0.15Li_2O$•MnO_2 partially occupy their sites, the structure can accommodate additional

lithium. During the electrochemical reduction of $0.15Li_2O{\bullet}MnO_2$, it is believed that the narrow (1 x 1) channels do not accommodate any significant amount of lithium and, therefore, do not contribute significantly to the electrode capacity.

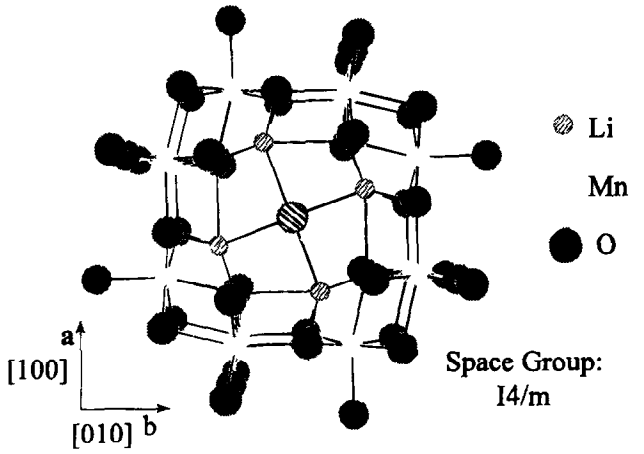

Fig. 19.

The structure of lithia-stabilized α-MnO_2, $0.15Li_2O{\bullet}MnO_2$ [107].

In principle, the tetragonal symmetry of the α-MnO_2 structure offers the possibility of designing an electrode which might be more tolerant to the Jahn-Teller effect than cubic lithium-manganese-oxide spinel structures (see section 3.1). For example, the Jahn-Teller effect in lithiated $Li_{1+x}[Mn_2]O_4$ is accommodated in one-dimension by a change in crystal symmetry from cubic to tetragonal during which the *c/a* ratio increases by 16% [16]. By contrast, the Jahn-Teller effect in lithiated Li_xMnO_2 (α) structures with tetragonal symmetry can be accommodated in two-dimensions, along the *a* and *b* directions of the unit cell, thereby offering greater tolerance to lithium insertion/extraction reactions [107].

The electrochemical discharge profiles for the first 12 cycles (3.8 to 2.0 V) of a $Li/0.15Li_2O{\bullet}MnO_2$ cell are shown in Fig. 20a [107]. Lithia-stabilized $0.15Li_2O{\bullet}MnO_2$ electrodes provide a significantly higher capacity and superior capacity retention on cycling compared to unstabilized α-MnO_2 electrodes (Fig. 20b). Nevertheless, the slow deterioration in performance that is observed with $0.15Li_2O{\bullet}MnO_2$ electrodes (synthesized from α-$MnO_2{\bullet}nH_2O$ materials) indicates that more work is required to enhance the structural stability of these electrodes even further to electrochemical cycling. In this regard, it must be noted that when lithium-stabilized α-MnO_2 electrodes are fabricated from $NH_4Mn_8O_{16}$ precursors, structures with lower crystallinity are produced which yield slightly higher capacities (170mAh/g) and superior stability to electrochemical cycling [108].

a)

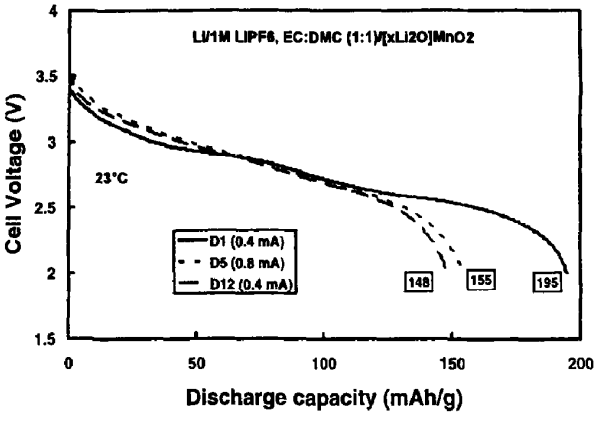

Fig. 20a.

The electrochemical behavior of various α-MnO_2 electrodes in non-aqueous lithium cells: (a) the first 12 cycles of a Li/0.15Li_2O•MnO_2 cell.

(b)

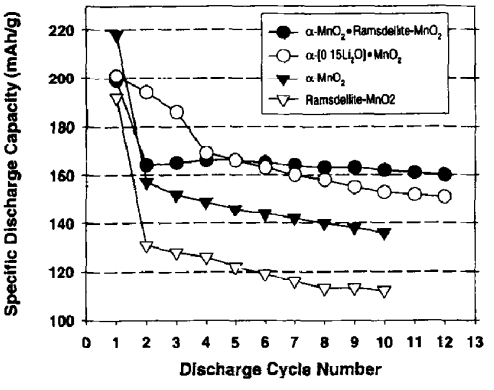

Fig. 20b.

Capacity (3.8 to 2.0 V) vs. cycle number for lithium cells with (i) α-MnO_2, (ii) 0.15Li_2O•MnO_2, (iii) ramsdellite-MnO_2, and (iv) α-MnO_2•ramsdellite-MnO_2 electrodes [107, 112].

The cyclic voltammograms of a pure α-MnO_2 electrode and a lithia-stabilized 0.15Li_2O•MnO_2 electrode are shown in Fig. 21a and b, respectively. It is clear that the initial lithium insertion into the α-MnO_2 structure occurs in two discrete steps. Although these two steps are more clearly resolved in the cyclic voltammogram of the pure, anhydrous α-MnO_2 electrode, good reversibility is only achieved on the first cycle; the peaks converge on subsequent cycling, which is consistent with the proposed structural change from the α-MnO_2 framework structure to a defect rock salt structure described in section 3.3.1. The two-step process in these materials can be readily understood: the first (high voltage) step can be attributed to a single-phase process during which lithium is inserted into the α-MnO_2 framework (or modified framework) to a composition $Li_{0.5}MnO_2$; the second step can be attributed to a possible two-phase reaction that could result from the anticipated Jahn-Teller distortion in the electrode particles when the average manganese oxidation state reaches ~3.5. This two-step reaction is clearly identified by the inflection in the initial discharge curve of the Li/0.15Li_2O•MnO_2 cell (Fig. 20a). Surprisingly, this point of inflection is not clearly evident in the initial discharge profile of the Li/α-MnO_2 cell (Fig. 17b). In this case, the onset of the second

step of the reaction appears to be associated with the slight change in the slope of the voltage profile (indicated by an arrow in Fig. 17a).

a)

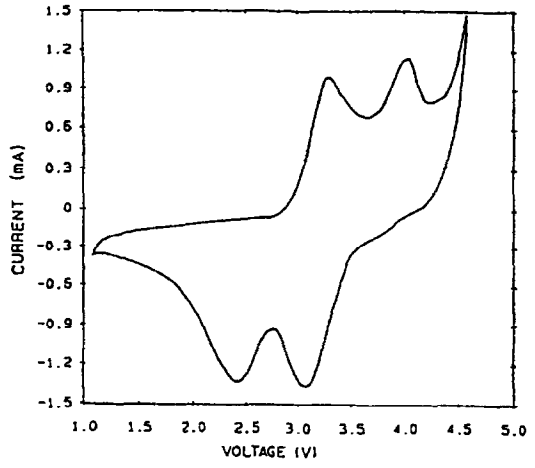

Fig. 21a.

The cyclic voltammograms of a pure anhydrous α-MnO_2 electrode in a liquid electrolyte cell at room temperature

b)

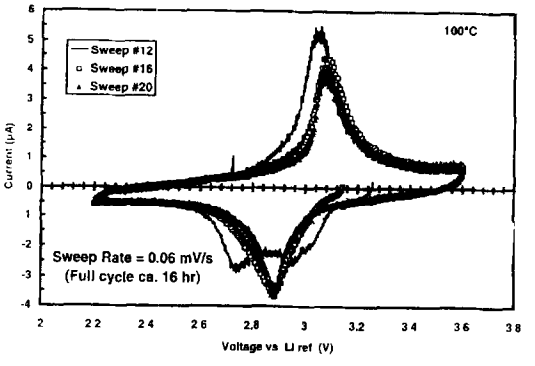

Fig. 21b.

A lithia-stabilized $0.15Li_2O{\cdot}MnO_2$ electrode in a polymer electrolyte cell at 100 °C [105, 107].

3.3.3 Ramsdellite-Stabilized α-MnO_2 Electrodes. When Mn_2O_3 is reacted with concentrated H_2SO_4 for prolonged periods of time, X-ray diffraction data of the products have shown that the α-MnO_2 structure first formed partially converts to a ramsdellite-MnO_2 structure (Fig. 22a) [112]. The ideal ramsdellite-MnO_2 structure (Fig. 22b) which is discussed in greater detail in section 3.5.2 has double chains of MnO_6 octahedra with an interstitial space comprised of channels with relative dimension (2 x 1). It appears, therefore, that under prolonged conditions of acid treatment, the large (2 x 2) channeis in the α-MnO_2 structure collapse to channels of smaller dimension. Information that has been obtained by transmission electron microscopy and convergent beam electron diffraction measurements has indicated that these products have grains of α-MnO_2, grains of ramsdellite-MnO_2 and grains of interconnected α-MnO_2 and ramsdellite-MnO_2 [112]. Electrodes fabricated from these composite electrode materials have shown good capacity retention (~160mAh/g) (Fig. 20b). These data endorse the

finding that the α-MnO_2 structure, *per se*, is inherently unstable and that it must be stabilized either by introducing some oxygen into the (2 x 2) channels or by connections to MnO_2 structures with smaller channel dimensions in order to withstand the repeated insertion and extraction of lithium during electrochemical cycling.

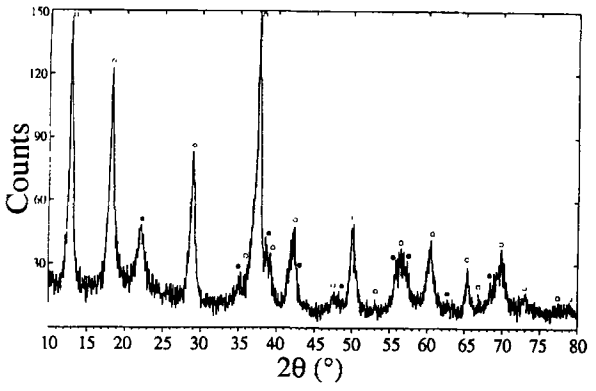

Fig. 22a.

The powder X-ray diffraction pattern of an α-MnO_2•ramsdellite-MnO_2 composite structure (○ = α-MnO_2, ● = ramsdellite-MnO_2) [10].

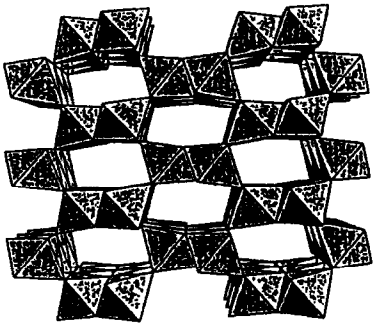

Fig. 22b. The structure of Ramsdellite-MnO_2. [10].

3.4 Beta-MnO_2

3.4.1 β-MnO_2 Electrodes. The structure of β-MnO_2 is shown in Fig. 23; it has a rutile-type structure with tetragonal symmetry ($P4_2/mnm$) [113]. The oxygen ions form a distorted hexagonal-close-packed array, (in rutile, sometimes referred to as tetragonal-close packing [114]. Single strands of edge-sharing MnO_6 octahedra propagate in a direction parallel to the crystallographic *c* axis. The interstitial space consists of unidimensional channels with relative dimension (1 x 1). Because the oxygen array is hexagonally-close packed, the octahedra in the interstitial space share faces with the MnO_6 octahedra. This structural property and the availability of only narrow one-dimensional channels for lithium-ion diffusion, makes β-MnO_2 unsuitable as an insertion electrode for lithium batteries; a highly crystalline β-MnO_2 structure can accommodate only 0.2 Li^+ ions at room temperature [115]. It has been shown that further

lithiation, for example, with a strong reducing agent such as n-butyllithium at 50°C is possible [113]. This reaction results in a shear of the oxygen array to cubic close-packing in response to the increasing electrostatic interactions between lithium and manganese ions which are located in face-shared octahedra in the lithiated β-MnO_2 structure. This process is accompanied by a cooperative displacement of one-half of the manganese ions into neighboring interstitial octahedral sites which transforms the rutile structure of β-MnO_2 to the $[Mn_2]O_4$ framework of a $Li_x[Mn_2]O_4$ spinel . A schematic representation of the rutile to spinel transformation is shown in Fig. 24 [113].

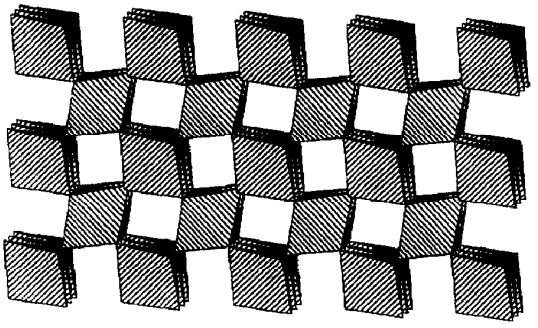

Fig. 23.
The structure of β-MnO_2 [13].

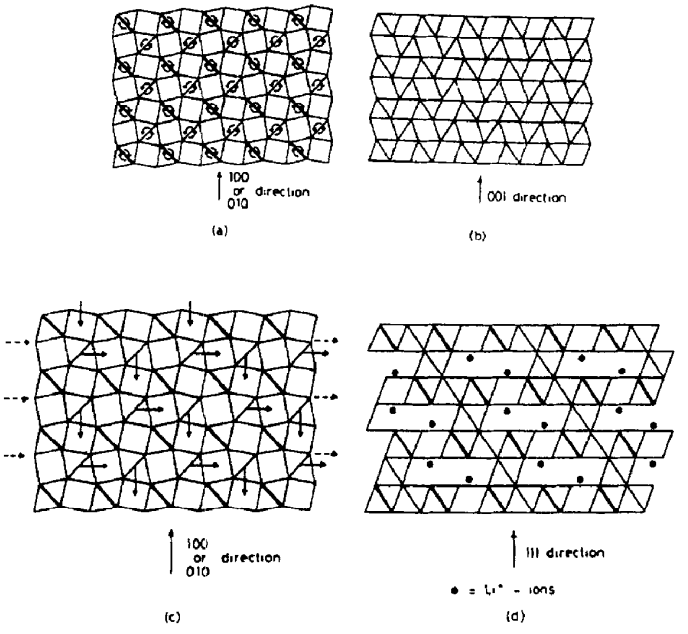

Fig. 24. A schematic representation for the transformation of β-MnO_2 (rutile-type structure) to a $Li_x[Mn_2]O_4$ spinel structure. Projection of (a) β-MnO_2, down the *c*-axis with Mn located in MnO_6 octahedra, (b) hexagonal-close-packed anion array derived from β-MnO_2, (c) β-MnO_2 and (d) $Li[Mn_2]O_4$ spinel. Curved arrows in (a) indicate rotations to (b), straight arrows in (c) indicate Mn displacements to reach (d), broken arrows in (c) indicate a shear direction [113].

The electrochemical profiles of Li/β-MnO_2 cells are shown in Fig. 25 [116]. Highly crystalline β-MnO_2 products with sharp X-ray diffraction patterns, for example, those prepared by thermal decomposition of $Mn(NO_3)_2$ at 400°C do not provide much capacity. By contrast, β-MnO_2 products that have poorly defined X-ray diffraction patterns, such as those prepared by heating a γ-MnO_2 product (derived from acid digestion of $Li[Mn_2]O_4$) to 300°C, can deliver a high initial capacity (210 mAh/g) at ~3 V in lithium cells. The high capacity has been attributed to the lower crystallinity of the β-MnO_2 particles (of average size 7 μm) which are strained and which have high surface area [116]. However, these electrodes do not cycle well; X-ray diffraction analyses of cycled electrodes have revealed "amorphous" products which indicate a degradation of the rutile structure. The poor cycling behavior suggests that an electrochemical transformation of β-MnO_2 to the $Li_x[Mn_2]O_4$ spinel structure takes place (consistent with the chemical transformation), because it has been well documented that $Li_x[Mn_2]O_4$ spinel electrodes do not cycle well at 3 V (see section 3.1).

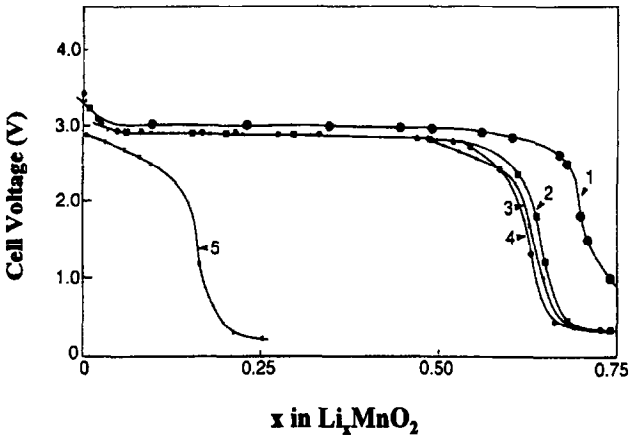

Fig. 25. Discharge characteristics of various Li/MnO_2 cells (30 μA cm^{-2}): 1, poorly crystalline β-MnO_2, prepared at 300°C; 2. β-MnO_2, prepared at 420°C; 3. EMD heated at 350°C; 4. EMD heated at 420°C; 5. highly crystalline β-MnO_2, prepared by decomposition of $Mn(NO_3)_2$ at 400°C [116].

3.5 Gamma-MnO_2 and Ramsdellite-MnO_2

3.5.1 γ-MnO_2 Electrodes. Of all the MnO_2 structures, γ-MnO_2 is the best known as an electrode material by the battery industry. γ-MnO_2 is used predominantly in aqueous Zn/MnO_2 cells, and in primary Li/MnO_2 cells [2, 117]. It has an intergrowth structure which contains β-MnO_2 domains of relative size (1 x 1), and ramsdellite-MnO_2 domains of size (2 x 1) (Fig. 26). The intergrowth structure can be adequately described in terms of de Wolff

disorder (the fraction of rutile-MnO_2 and ramsdellite-MnO_2 domains in the sample) and microtwinning to account for the variation in peak widths and intensities in the powder X-ray diffraction patterns of γ-MnO_2 materials. γ-MnO_2 materials can be prepared by either electrolytic techniques (EMD) (Fig. 27a) or by chemical methods (CMD) (Fig. 27b). In both cases, the γ-MnO_2 products contain water which is located at grain boundaries and occluded within the structure. For lithium battery applications, which require anhydrous materials, γ-MnO_2 products must be heated at 350-400°C to remove the water content [118]. Heat-treatment slightly increases the concentration of β-MnO_2 domains in the structure which reduces the ability for the structure to accommodate lithium and, therefore, its electrode capacity. The oxygen lattice of γ-MnO_2 , like β-MnO_2, has a distorted hexagonally-close-packed arrangement which expands considerably during lithium insertion [14, 119]. During discharge, lithium ions are inserted predominantly into the larger (2 x 1) channels of the ramsdellite domains. Although high discharge capacities, up to 250 mAh/g are achievable on the initial discharge at low current rates, γ-MnO_2 electrodes lose capacity on electrochemical cycling (Fig. 28) [119].

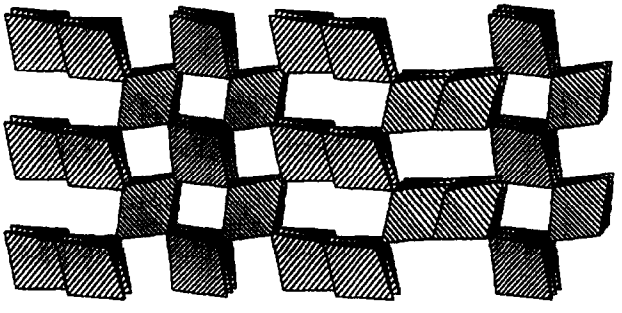

Fig. 26.

The structure of γ-MnO_2 [13].

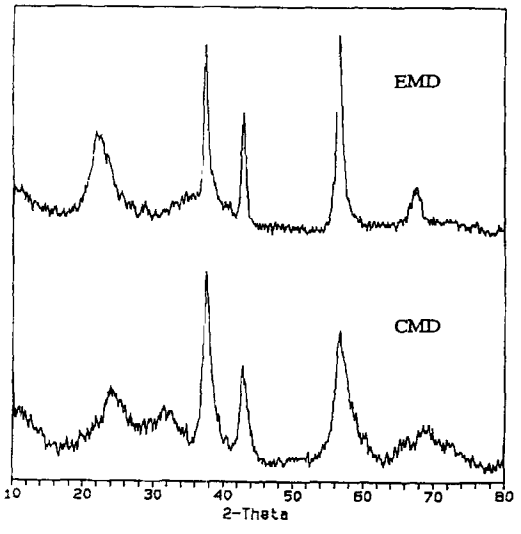

Fig. 27.

The powder X-ray diffraction patterns of a typical γ-MnO_2 products, (a) EMD and (b) CMD [10].

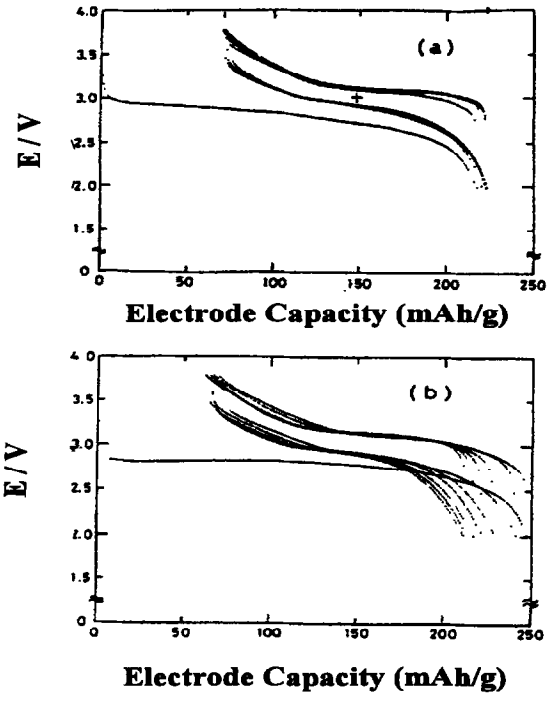

Fig. 28.

The electrochemical cycling behavior of Li/γ-MnO_2 cells between 2.0 and 3.8 V (0.17 mA/cm^2): (a) EMD heated at 250°C, (b) EMD heated at 400°C [14].

It is difficult to obtain accurate information about the structural modifications that occur when γ-MnO_2 products are lithiated because of the complexity of interpreting the X-ray patterns of intergrown, poorly developed γ-MnO_2 structures. However, with the synthesis of highly crystalline ramsdellite-MnO_2 materials, it has been possible to obtain information which has provided an insight into the structural behavior of γ-MnO_2 electrodes which limits their stability to electrochemical cycling.

3.5.2 Ramsdellite-MnO_2 Electrodes: the Ramsdellite-MnO_2 to Spinel Transformation. Highly crystalline ramsdellite-MnO_2 materials (i.e. γ-MnO_2 structures with a very low fraction of β-MnO_2 domains) that have relatively sharp and well resolved peaks in their X-ray diffraction patterns (Fig. 29a) can be prepared by the acid digestion of the spinel $Li[Mn_2]O_4$ under carefully controlled conditions [120]. Lithiation with a strong reducing agent such as n-butyllithium at room temperature tends to destroy the structural integrity of the ramsdellite framework as shown by the broadening and collapse of the X-ray diffraction peaks [10], whereas lithiation with a relatively mild reducing agent such as lithium iodide in acetonitrile at 80°C preserves the crystalline structure up to a composition $Li_{0.9}MnO_2$

(Fig. 29b-d) [120]. Structural refinements of ramsdellite-MnO_2 and its lithiated products have shown that the hexagonally-close-packed array of the parent material shears on lithiation toward cubic close-packing in response to the increasing electrostatic interactions between the incoming lithium ions and the manganese ions. The result is a severe buckling of the structure as shown in Figs. 30 (a-c) [120]. The orthorhombic unit cell (space-group Pnam) expands anisotropically during this process (Table 2); the lattice parameters in $Li_{0.9}MnO_2$ reflect a 5.6% increase in a, a 16.5% increase in b, and a 1% decrease in c, and an overall expansion of the unit cell of 21.4%. These changes in unit cell parameters, particularly the large increase in b are undoubtedly too severe for the ramsdellite-MnO_2 structure, and by analogy the γ-MnO_2 structure, to maintain structural integrity over prolonged electrochemical cycling of lithium.

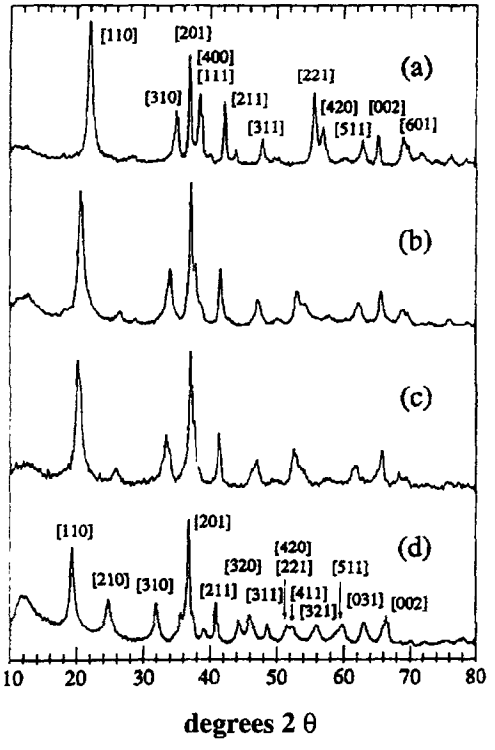

Fig. 29.

The powder X-ray diffraction patterns of (a) ramsdellite MnO_2, (b) $Li_{0.3}MnO_2$, (c) $Li_{0.5}MnO_2$, and (d) $Li_{0.9}MnO_2$ [120].

Table 2. Crystallographic parameters of ramsdellite (R)-MnO_2 and lithiated products [120] (Space Group = Pnam)

Compound	***a*** **(Å)**	***b*** **(Å)**	***c*** **(Å)**	**Volume (Å^3)**	**Volume Expansion**
R-MnO_2	9.372 (2)	4.471 (1)	2.851 (1)	119.5 (1)	-
$Li_{0.5}MnO_2$	9.501 (4)	4.985 (3)	2.841 (1)	134.6 (2)	12.6
$Li_{0.9}MnO_2$	9.910 (5)	5.208 (3)	2.812 (1)	145.1 (2)	21.4

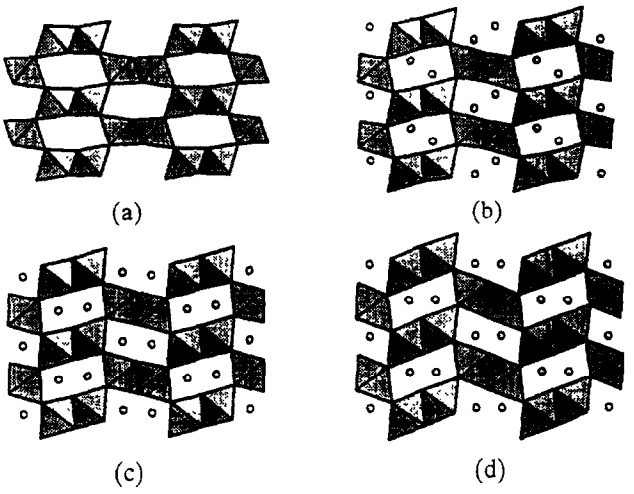

Fig. 30.

The structures of
(a) ramsdellite-MnO_2, and its lithiated products:
(b) $Li_{0.5}MnO_2$,
(c) $Li_{0.5}MnO_2$, and
(d) $Li_{0.9}MnO_2$. Shaded octahedra contain $Mn^{4+/3+}$ ions, o = Li^+ ions [120].

Lithiated ramsdellite-MnO_2 materials transform readily to spinel-type structures when they are heated at moderate temperatures [120]. When heated under inert conditions, for example, under vacuum, the lithiated ramsdellite-MnO_2 product, $Li_{0.5}MnO_2$ transforms readily to the spinel $Li[Mn_2]O_4$ at 300°C (Fig. 31(a,b)). If the heating is conducted in air, the $Li_{0.5}MnO_2$ phase is oxidized and transforms sluggishly to the oxygen-rich spinel $Li_2Mn_4O_9$ ($LiMn_2O_{4.5}$) (Fig. 31(c-f). A model for the ramsdellite-MnO_2 to $Li[Mn_2]O_4$ spinel phase transformation is given in Fig. 32 [120]; it involves an initial shear of the oxygen array to cubic close-packing and a displacement of 50% of the manganese ions into neighboring interstitial octahedra.

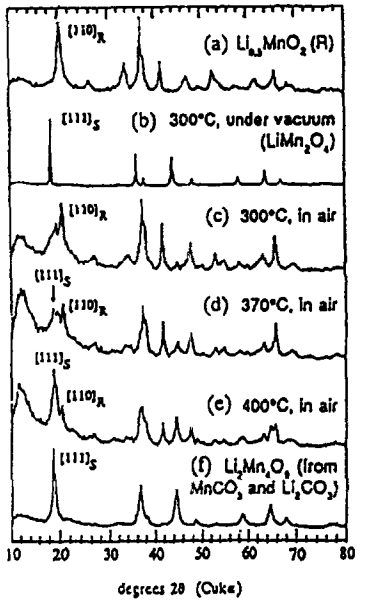

Fig. 31.

The powder X-ray diffraction patterns of (a) lithiated ramsdellite-MnO_2 of composition $Li_{0.5}MnO_2$, (b) after heating $Li_{0.5}MnO_2$ under vacuum at 300°C, (c-e), after heating $Li_{0.5}MnO_2$ in air at 300, 370 and 400°C, and (f) $Li_2Mn_4O_9$ prepared from $MnCO_3$ and Li_2CO_3 at 400°C. (R = ramsdellite-MnO_2 peaks, S = spinel peaks) [120].

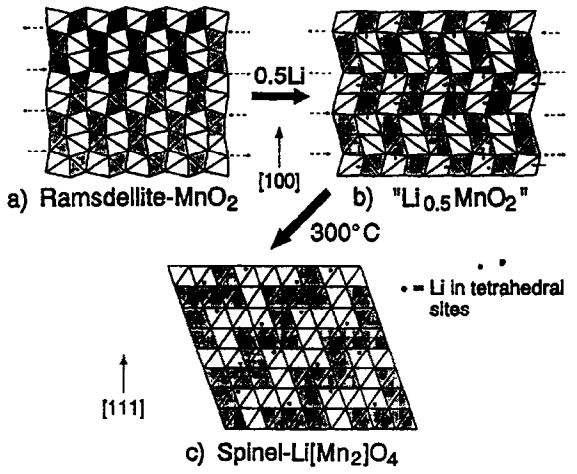

Fig. 32.

A schematic representation for the transformation of lithiated-ramsdellite $Li_{0.5}MnO_2$ to spinel $Li[Mn_2]O_4$ [120].

3.5.3 Lithia-stabilized γ-MnO_2 and ramsdellite-MnO_2 electrodes ("CDMO" products). Gamma-MnO_2 and ramsdellite-MnO_2 compounds that are prelithiated by reaction with LiOH or $LiNO_3$ at 300 - 400°C in air have been shown to provide improved electrochemical cycling compared to their parent γ-MnO_2 and ramsdellite-MnO_2 structures [121-130]. Nohma et al. determined that the optimum Li:Mn ratio to use was 3:7 (1:2.33) [128]; the ratio is close to that found in spinel compounds such as $Li[Mn_2]O_4$ and $Li_2Mn_4O_9$ (Li:Mn = 1:2). These prelithiated compounds tend to consist of two-phases; a lithiated γ-MnO_2 (ramsdellite-MnO_2) phase and a spinel-related phase [4, 120, 131]; the overall product is commonly referred to by the acronym "CDMO" (Composite Dimensional Manganese Dioxide) after Sanyo. The powder X-ray diffraction pattern of a typical CDMO product is shown in Fig. 33; it is similar to the X-ray diffraction patterns of the heated lithiated-ramsdellite-MnO_2 products shown in Fig. 31d. In practice, these CDMO materials are slightly oxygen-deficient and can be represented by the general formula $Li_3Mn_7O_{15\ 5-\delta}$ in which δ is small. For a fully-oxidized state (δ = 0), CDMO products could be represented as $0.21Li_2O{\bullet}MnO_2$.

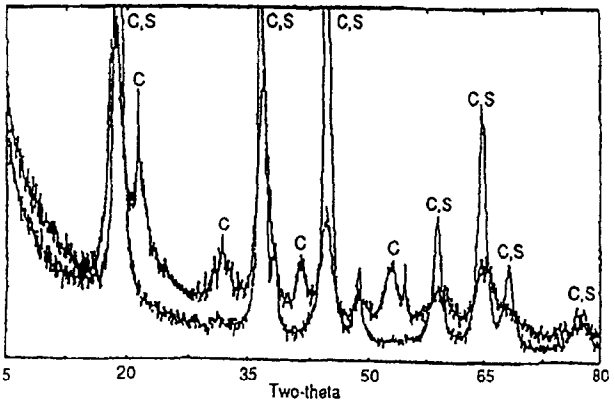

Fig. 33.

The powder X-ray diffraction pattern of a typical CDMO product [10]. The pattern has peaks which are coincident with those of an oxygen-rich spinel phase (S), such as $Li_2Mn_4O_9$, and a lithiated-MnO_2 phase derived from γ-MnO_2 (C).

The limiting composition of the lithia-stabilized ramsdellite-MnO_2 component has been determined by reaction of ramsdellite-MnO_2 and $LiNO_3$ at 300°C to be approximately $0.15Li_2O{\bullet}MnO_2$, (i.e. with Li:Mn = 0.3:1.0) assuming fully oxidized manganese ions. The structure of the lithia-stabilized ramsdellite-MnO_2 structure $0.15Li_2O{\bullet}MnO_2$, is shown in Fig. 34 [10]. The incorporation of Li_2O in the ramsdellite-MnO_2 structure increases the ratio of cations to anions in the structure. The result is a buckling of the hexagonal close-packed oxygen array and a transformation to a cubic-close-packed structure, similar to lithiated ramsdellite-MnO_2 products obtained by lithiation with n-butyllithium or lithium iodide (Figs. 30 (b,c)). It is of interest to note that the composition, $0.15Li_2O{\bullet}MnO_2$, coincides with the concentration of Li_2O which is also required to stabilize the α-MnO_2 structure (see section 3.3).

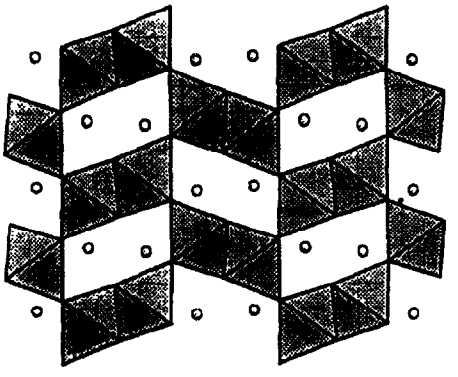

Fig. 34.

The structure of lithia-stabilized ramsdellite-MnO_2, $0.15Li_2O{\bullet}MnO_2$. Shaded octahedra contain Mn^{4+} ions, o = Li^+ ions [10].

Examination of the Li-Mn-O phase diagram shows that the composition of a fully-oxidized CDMO products ($0.21Li_2O{\bullet}MnO_2$) would fall between the composition of a lithiated γ-MnO_2 (ramsdellite-MnO_2) phase of nominal stoichiometry $0.15Li_2O{\bullet}MnO_2$ and the spinel phase $Li_4Mn_5O_{12}$ ($0.4Li_2O{\bullet}MnO_2$) (Fig. 1b)). Both components of CDMO products have close-

packed oxygen arrays which are either ideally cubic-close-packed (spinel phase) or which deviate slightly from ideal packing (lithiated γ-MnO_2 (ramsdellite-MnO_2) phase). Because of the compatibility between the oxygen arrays of the two components, it is easy to imagine that CDMO materials could have connected or intergrown structures. This concept has recently been confirmed in an examination of CDMO electrodes by high-resolution electron microscopy and by convergent beam electron diffraction methods [131]. In particular, the presence of the spinel domains in the intergrown structure is believed to play an important role in stabilizing the composite electrode to lithium insertion/extraction reactions [4].

The discharge profile of a typical Li/CDMO cell is shown in Fig. 35 [10]. The electrochemical reaction that occurs at approximately 3 V is consistent with the lithium occupation of octahedral sites in a rock salt-type structure; the reaction at higher voltage (~3.5 V vs. Li) is believed to be associated with lithium occupation of either tetrahedral or octahedral sites, and is dependent on the distribution of the manganese ions within the close-packed oxygen array. Excellent electrochemical performance has been reported for CDMO electrodes in coin cells; they can deliver a capacity of 200 mAh/g and show good rechargeability even if charged to a high potential (3.6 V vs LiAl) [128].

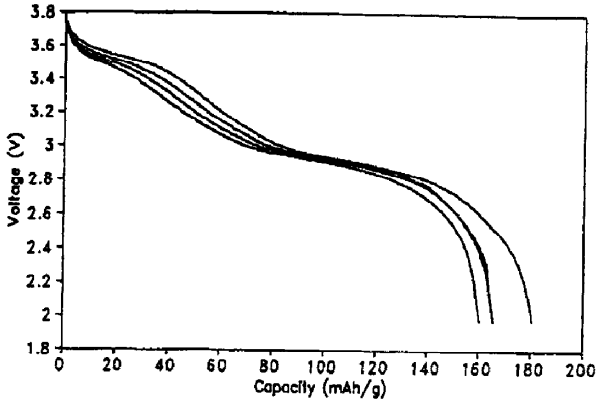

Fig. 35.

The discharge voltage profile of a typical Li/CDMO cell when cycled between 3.8 and 2.0 V (first four cycles) [10].

3.6. Layered-MnO_2 Compounds

Host electrodes with layered structures are of particular interest to the battery industry because they provide a two-dimensional interstitial space that allows for rapid lithium ion transport within the host. Of particular note are the layered compounds $LiCoO_2$ and $LiNiO_2$ (and compounds within the solid solution series $LiCo_{1-x}Ni_xO_2$ ($0 \le x \le 1$) whose structures can provide excellent stability to lithium insertion/extraction over a wide compositional range between 3.5 and 4.5 V vs. Li [11, 132-140]. These materials are currently being exploited as insertion electrodes in commercial lithium-ion cells. Because manganese oxides are generally accepted as being less expensive and less toxic than cobalt and nickel oxides, concerted efforts have been made in research laboratories to synthesize layered manganese oxide electrodes that might offer comparable performance to $LiCoO_2$ and $LiNiO_2$

3.6.1 Birnessite-type (δ)-MnO_2 Electrodes. Many layered manganese oxides (δ-MnO_2) exist in nature. They are commonly referred to as birnessite-type compounds (after the mineral *birnessite*) or as phyllomanganates. These materials can be prepared synthetically by "low temperature" methods, for example, by oxidation reactions in alkaline solution [141-143], reduction of permanganates in acid [142-149] or by hydrothermal methods [150] The initial products usually contain a significant amount of water and stabilizing cations such as Na^+ or K^+ between the sheets of MnO_6 octahedra. Lithium analogues can be prepared by ion-exchange reactions [151-152]. The birnessite compounds have an interlayer separation of approximately 7 Å. In general, it has proven difficult to remove all the water from these materials without degradation of the layered structure. Nevertheless, with careful heating, to moderate temperature (e.g. 80 - 250°C [141, 151] it has been demonstrated that much of the layered character of the MnO_2 structure can be maintained. These partially dehydrated materials can deliver high capacities on the initial discharge, up to 0.7 Li per Mn (>200 mAh/g), and show sloping discharge profiles between 4 V and 2 V (Fig. 36). In general, these materials do not cycle well, and capacity retention is poor. These materials, therefore, appear to be of limited interest for lithium battery applications.

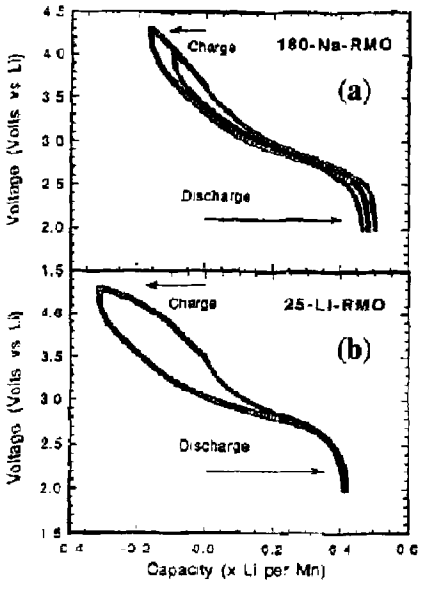

Fig. 36.

The voltage profile for lithium insertion/extraction reactions at the first charge-discharge cycle for layered rancieite electrodes, (a) a sodium-rancieite structure of composition $Na_{0.33}MnO_2 \cdot 0.10H_2O$ (180°C heat-treatment), and (b) an ion-exchanged lithium-rancieite structure of composition $Li_{0.42}MnO_2 \cdot 1.06H_2O$ (no heat-treatment) [148].

3.6.2 Layered-MnO_2 from Li_2MnO_3. The realization that it was possible to leach Li_2O from the defect spinel $Li_2Mn_4O_9$ ($Li_2O \cdot 4MnO_2$), or in spinel notation, $(Li_{0.89}\square_{0.11})_{8a}[Mn_{1.78}\square_{0.22}]_{16d}O_4$, by acid treatment to yield the spinel framework $[Mn_2]O_4$ (λ-MnO_2), prompted efforts to synthesize a layered MnO_2 compound by acid digestion of the layered rock salt structure, Li_2MnO_3 ($Li_2O \cdot MnO_2$) [153-154]. The structure of Li_2MnO_3 is depicted in Fig. 37; it has monoclinic symmetry, C2/m). The structure has a close-packed oxygen array which is slightly distorted from ideal cubic-close-packing. Layers of lithium ions and layers of lithium and manganese ions (in a 1:2 ratio) alternate between the close-packed oxygen planes. The Li_2MnO_3 structure is closely related to the layered structures of $LiCoO_2$ and $LiNiO_2$; it can be represented, in layered notation, as $\{Li\}_{3a}(Li_{0.33}Mn_{0.67})_{3b}O_2$ in which 3a and 3b refer to the octahedral sites of the trigonal space group R3m that are occupied by the lithium and Co and Ni ions in $LiCoO_2$ and $LiNiO_2$, respectively. Li_2MnO_3 is electrochemically inactive; lithium cannot be inserted into the structure because all the octahedral sites are fully occupied, neither can lithium be extracted from the structure because all the manganese ions are tetravalent and cannot be oxidized further. However, removal of Li_2O from Li_2MnO_3 without displacing the manganese cations from their layers could, in principle, yield an electrochemically-active, layered MnO_2 structure with a cubic-close-packed oxygen array. This reaction, in layered notation, can be represented:

$$3/2\ \{Li\}_{3a}(Li_{0.33}Mn_{0.67})_{3b}O_2 - Li_2O \rightarrow (Mn)_{3b}O_2 \quad (7)$$

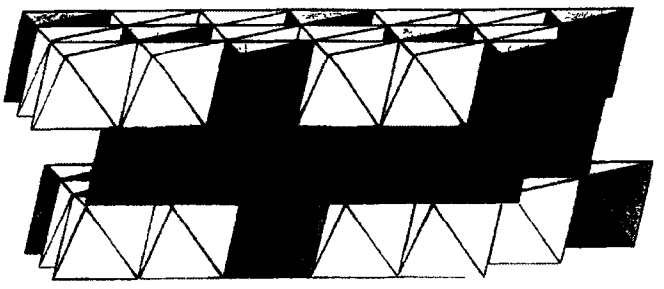

Fig. 37.

The structure of Li_2MnO_3 (rock salt) [153].

Li_2MnO_3 can be prepared as a highly crystalline material at 850°C. Reaction with concentrated acid gradually leaches Li_2O from the structure to leave a two-phase product consisting of extensively delithiated $Li_{2-x}MnO_{3-x/2}$ particles with a defect rocksalt (layered structure) at the surface and "unreacted" Li_2MnO_3 within the bulk as shown by the X-ray diffraction patterns in Fig. 38(a,b) [10]. Heat-treatment of the two-phase $Li_{2-x}MnO_{3-x/2}$ product, with $x \approx 1$, at 300°C yields an X-ray diffraction pattern which resembles that of the parent material (Fig. 38c) [10, 155]. Close examination of the X-ray pattern indicates that the heat-treatment step destroys the layered phase which reacts with the unreacted Li_2MnO_3 component causing a displacement of some manganese ions into the lithium depleted layers to yield a product with some spinel-like character [153]. The averaged structure of $Li_{2-x}MnO_{3-x/2}$ products, therefore, can be considered to have a manganese-ion distribution which is intermediate between that of a layered structure and a spinel structure. From an electrochemical viewpoint, these materials show voltage profiles similar to spinels, discharging most of their capacity at constant voltage at approximately 3 V vs lithium (Fig. 39) [154].

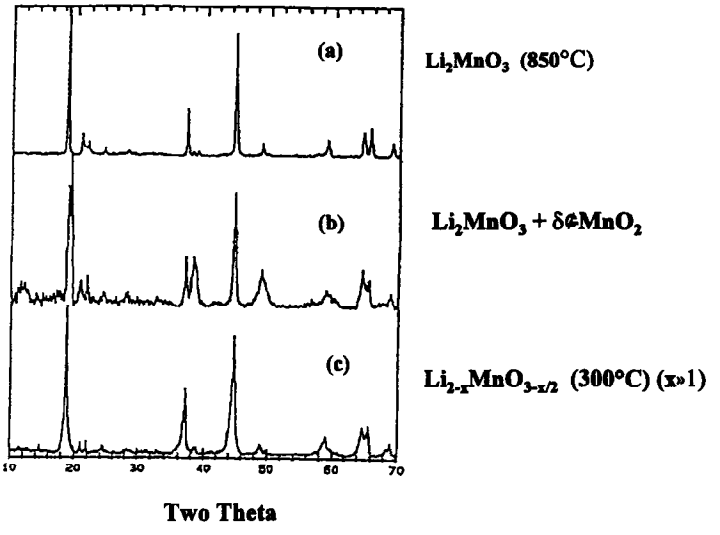

Fig. 38. The powder X-ray diffraction patterns of $Li_{2-x}MnO_{3-x/2}$ products derived from Li_2MnO_3 (850°C preparation). (a) parent material (x = 0), (b) a two-phase product with x≈1, (c) a "single-phase" product after heating (b) to 300°C in air [10].

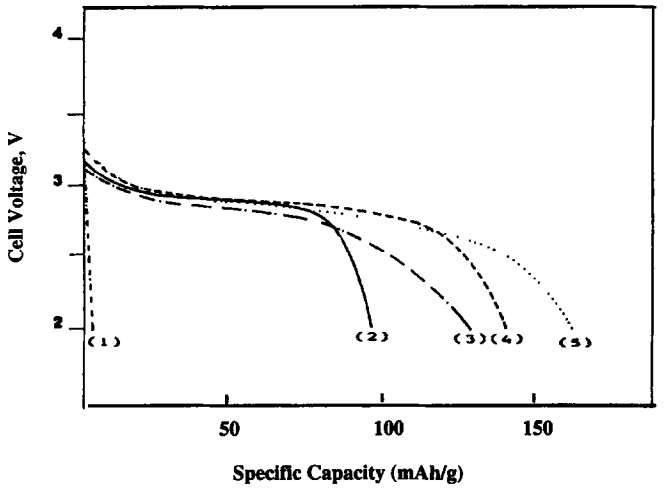

Fig. 39. The electrochemical discharge profiles of Li/$Li_{2-x}MnO_{3-x/2}$ cells, (1) x = 0, (2) x = 0.84, (3) x = 1.2, (4) x = 1.4 and (5) x = 1.58 [154].

When Li_2MnO_3 is synthesized at a moderate temperature, such as 400°C, the product is less crystalline and more reactive to concentrated acid than the highly crystalline compounds prepared at higher temperature. When subjected to acid treatment, most of the lithium can be

removed from the structure; an x = 1.85 in $Li_{2-x}MnO_{3-x/2}$, corresponding to a composition $Li_{0.14}Mn_{0.96}O_2$ has been reported [153]. The X-ray diffraction patterns of the (400°C) parent material, a delithiated compound, in layered notation, $Li_{0.36}Mn_{0.91}O_2$ corresponding to x = 1.64 in $Li_{2-x}MnO_{3-x/2}$, and a relithiated product, $Li_{1.09}Mn_{0.91}O_2$, obtained by chemically lithiating $Li_{0.36}Mn_{0.91}O_2$ with LiI at room temperature, are shown in Figs. 40(a-c) [156]. A structure analysis of the delithiated product has shown that removal of lithia from Li_2MnO_3 results in a shear of the cubic-close-packed oxygen planes to create a structure with alternate layers of octahedra and trigonal prisms (Fig. 41a). The manganese ions remain in alternate layers (in the octahedra) and are not displaced to the lithium layer during the leaching process; the residual lithium ions were assumed to be located in the octahedral sites not occupied by manganese and in some trigonal prismatic sites. Lithiation of $Li_{0.36}Mn_{0.91}O_2$ with LiI regenerates the cubic close packed oxygen array of the parent Li_2MnO_3 structure, but produces a rock salt structure $Li_{1.09}Mn_{0.91}O_2$ that closely-resembles that of $LiCoO_2$ and $LiNiO_2$ (Fig. 41b).

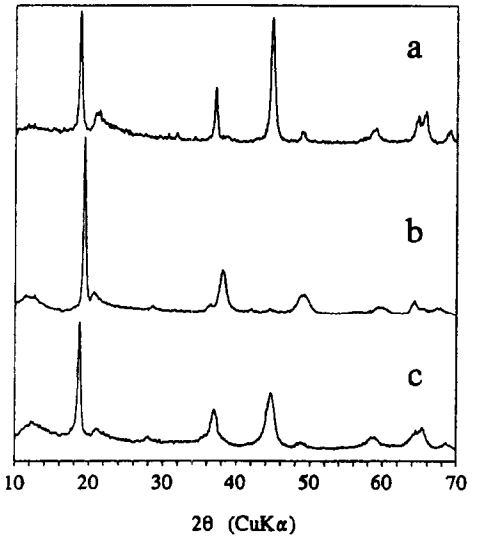

Fig. 40.
The powder X-ray diffraction patterns of (a) Li_2MnO_3 (400°C), (b) $Li_{0.36}Mn_{0.91}O_2$ and (c) $Li_{1.09}Mn_{0.91}O_2$ [156].

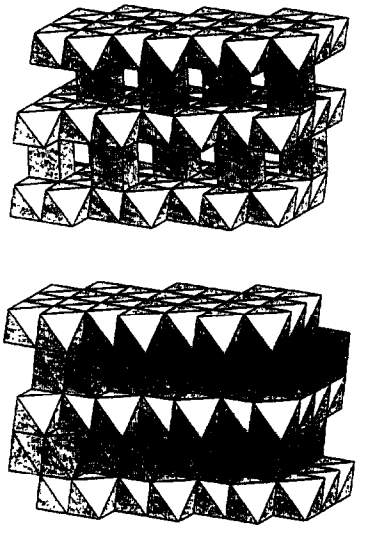

Fig. 41.
The layered structures of (a) $Li_{0.36}Mn_{0.91}O_2$, and (b)$Li_{1.09}Mn_{0.91}O_2$ [156].

Layered-$Li_{2-x}MnO_{3-x/2}$ structures are prepared under aqueous conditions and, therefore, tend to contain residual water at the grain boundaries which is difficult to remove completely. Highly delithiated samples are unstable to heat treatment and convert readily to γ/β-MnO_2-type structures at 300°C. The presence of water and the instability of the oxygen array to lithium insertion/extraction, has thus far, limited their application as electrodes for lithium cells. Like birnessite-type compounds, layered-$Li_{2-x}MnO_{3-x/2}$ electrode structures offer a high initial capacity (~200 mAh/g) but lose capacity steadily when cycled over the voltage range 3.8 to 2.0 V (Fig. 42) [153]. The cyclic voltammogram of a layered-$Li_{2-x}MnO_{3-x/2}$ electrode with composition $Li_{0.14}Mn_{0.96}O_2$ (corresponding to x = 1.85) is shown in Fig. 43a [153]; it has a profile similar to that of a γ-MnO_2 electrode and suggests that the reduction peak at approximately 2.7 V corresponds to the insertion of lithium into octahedral sites between sheets of MnO_6 octahedra. Although capacity is lost on the initial cycle, the cyclic voltammogram indicates that the process is at last partially reversible. The cyclic voltammogram of a $Li_{2-x}MnO_{3-x/2}$ electrode with composition $Li_{0.65}Mn_{0.84}O_2$ (corresponding to x = 1.22) that had been heated to 300°C has features of a spinel electrode; it shows an additional reduction process at 4 V, indicative of the insertion of lithium into tetrahedral sites (Fig. 43b).

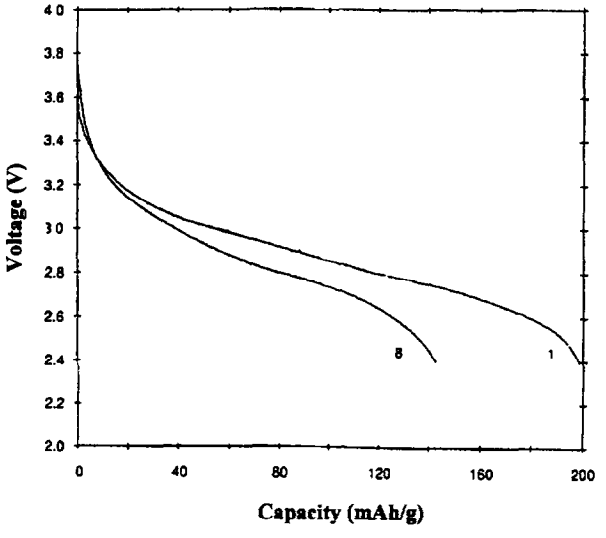

Fig. 42.

The electrochemical voltage profiles on the initial and eighth discharge of a Li/$Li_{2-x}MnO_{3-x/2}$ cell (x = 1.85) [153].

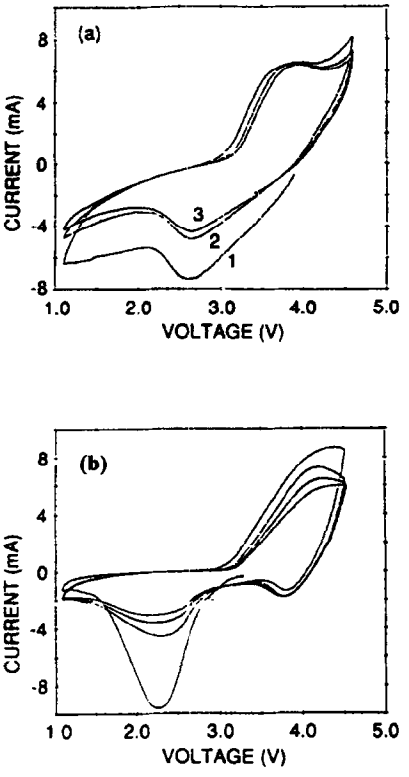

Fig. 43.

Cyclic voltammograms of $Li/Li_{2-x}MnO_{3-x/2}$ electrodes in lithium cells, (a) layered structure (x = 1.85) and (b) heated sample (300°C, x = 1.22) showing spinel-type features at 4 V (scan rate = 1 mV s^{-1}) [153].

3.6.3 Layered-$LiMnO_2$ from $NaMnO_2$: The Layered-$LiMnO_2$ to Spinel Transition.

It has not yet been possible to prepare a $LiMnO_2$ compound that is isostructural with $LiCoO_2$ by conventional high temperature solid state reactions, nor has it been possible to prepare anhydrous layered-MnO_2 compounds from aqueous routes. Attempts to synthesize a layered $LiMnO_2$ structure therefore, turned to non-aqueous ion-exchange techniques using α-$NaMnO_2$ (which is isostructural with $LiCoO_2$) as a precursor. These attempts have been largely successful. The success of this technique is highly dependent on the temperature at which the ion-exchange process is carried out. For example, the ion exchange reaction of α-$NaMnO_2$ with molten LiI (460°C) results in the lithiated spinel $Li_2[Mn_2]O_4$; with molten LiBr (560°C) and molten LiCl (650°C), the product is a mixture of the lithiated spinel $Li_2[Mn_2]O_4$ and orthorhombic-$LiMnO_2$ [157]. However, by performing the reaction under reflux conditions at considerably lower temperature with LiCl or LiBr in hexanol at 145°C [158] or methanol [159, 160] (temperature not disclosed), it has been possible to obtain an almost ideal layered $LiMnO_2$ structure. The powder X-ray diffraction pattern of a typical layered-$LiMnO_2$ sample is shown in Fig. 44. Despite the difficulties of distinguishing between a layered $LiMO_2$ structure and a lithiated spinel

$Li_2[M_2]O_4$ (where M = metal cation, e.g. Co or Mn) [161], Rietveld refinements have shown that the structure is layered, but that between 3 and 9% manganese is present in the lithium layer. High resolution electron microscopy data and convergent beam electron diffraction measurements have shown that $LiMnO_2$ samples contain, predominantly, grains of the layered $LiMnO_2$ structure, but also some grains of the lithiated spinel phase $Li_2[Mn_2]O_4$; evidence of an intergrown structure has also been observed [162]. A schematic representation of the ideal $LiMO_2$ structure is shown in Fig. 45. Lithium is initially extracted from the structure between 3.2 and 4.2 V (Fig. 46) [159]. However, subsequent cycling of the cells has shown that very little capacity is recovered on discharge over this voltage range, but that on extending the voltage limits to 4.2 and 2.4 V some capacity can be recovered. Continual cycling over the extended voltage range shows a voltage profile that develops into one that is characteristic of a $Li_x[Mn_2]O_4$ spinel. (Fig. 46). This observation is consistent with Rietveld refinements of electrodes that clearly demonstrate that some of the manganese ions diffuse from their original layer into the lithium layer (note that the ratio of manganese in alternate layers in the spinel $Li[Mn_2]O_4$ is 3:1). This behavior is similar to that observed for layered $LiVO_2$, in which, on delithiation, approximately one-third of the vanadium ions diffuse from their layer to the lithium-deficient layer to yield a defect rock salt structure [163-164]. The instability of the layered $LiMnO_2$ structure to delithiation, therefore, limits its use as an electrode for lithium batteries, and endorses the stability of spinel-type structures in the Li-Mn-O system.

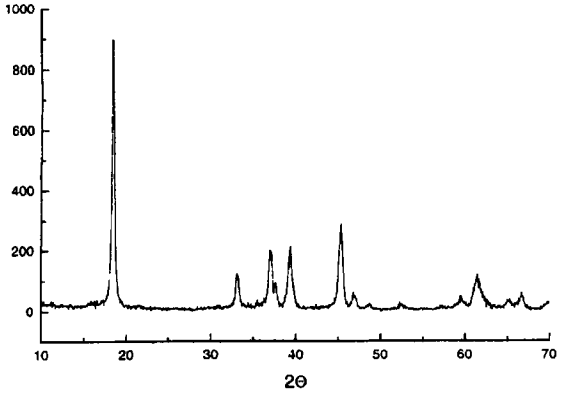

Fig. 44.

The powder X-ray diffraction pattern of a typical layered $LiMnO_2$ compound (The sample was kindly provided by R. Gitzendanner and P.G. Bruce).

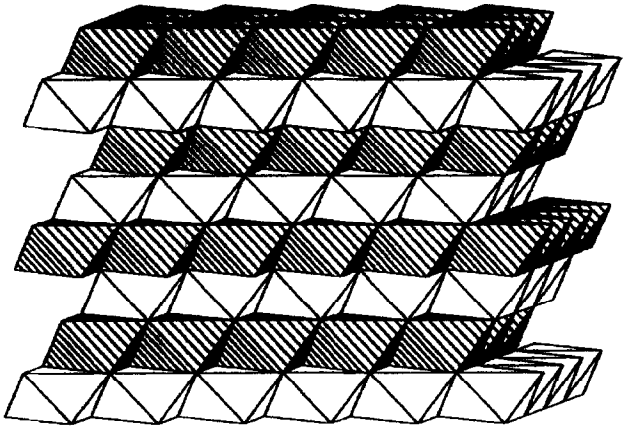

Fig. 45.

The ideal $LiMO_2$ structure (M = Co, Ni, V, Mn) [13].

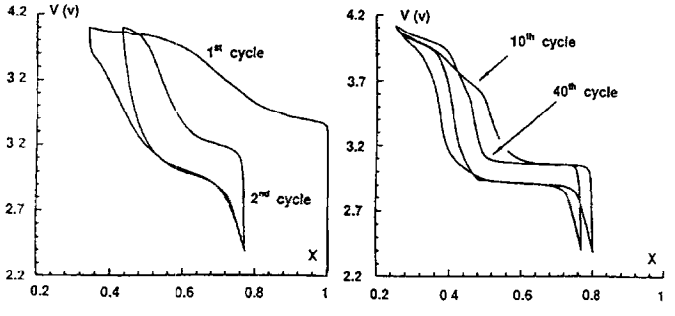

Fig. 46.

Electrochemical profiles for a Li/layered-Li_xMnO_2 cell [159].

3.7. Orthorhombic-$LiMnO_2$

3.7.1 Orthorhombic-$LiMnO_2$ Electrodes: The Orthorhombic-$LiMnO_2$ to Spinel Transformation. $LiMnO_2$ with orthorhombic symmetry (Pmnm) can be prepared in highly crystalline form by a conventional solid state reaction between Li_2CO_3 and MnO_2 at 800-1000°C under argon [165-166]. Orthorhombic-$LiMnO_2$ materials that are less crystalline can be prepared at lower temperature, for example, at 600°C by reducing MnO_2 in the presence of LiOH with carbon [167], or by reacting γ-MnOOH with LiOH under nitrogen or helium at 300-450°C [168-169]. An undisclosed method for preparing orthorhombic-$LiMnO_2$ has also been reported [170]. The structure of orthorhombic-$LiMnO_2$ is shown in Fig. 47 and its X-ray diffraction pattern in Fig. 48. It can be classified as rock salt structure in which the manganese and ions form independent sheets of MnO_6 and LiO_6 octahedra that are arranged in corrugated

(zig-zag) layers. The oxygen array is distorted from ideal cubic-close-packing by the Mn^{3+} (Jahn-Teller) ions. Although the structure is sometimes referred to as being layered, it must be noted that the corrugated layers of the MnO_6 and LiO_6 octahedra are not parallel to the close-packed oxygen layers as they are in layered-$LiMnO_2$ with monoclinic symmetry (section 3.6.3).

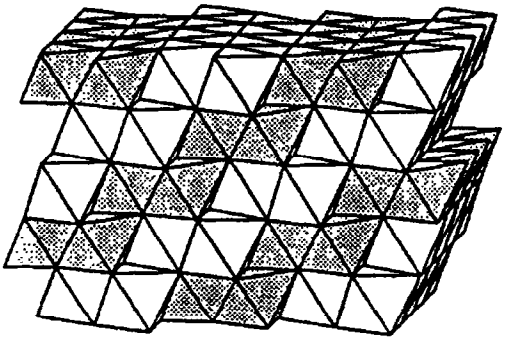

Fig. 47.

The structure of orthorhombic-$LiMnO_2$ [167].

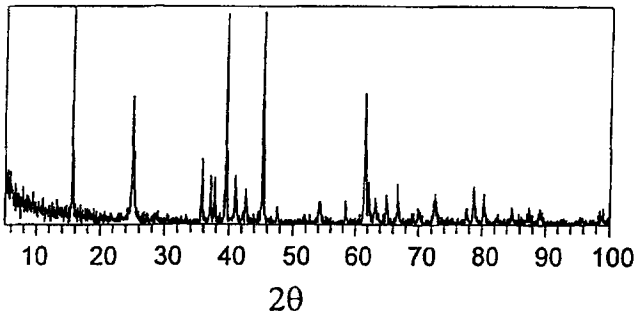

Fig. 48.

The powder X-ray pattern of orthorhombic $LiMnO_2$ synthesized at 800-1000 °C under argon [166].

Orthorhombic-$LiMnO_2$ electrode materials that are prepared at low to moderate temperature have high surface areas and small particle-size; they will tend to provide higher initial charge and discharge capacities than highly crystalline materials that are made at higher temperatures. The electrochemical behavior of a typical orthorhombic-$LiMnO_2$ electrode (prepared at 600 °C) is shown in Fig. 49a [167]. On the initial charge, approximately 75% of the lithium is extracted from the structure in a two-stage process between 3.4 and 4.5 V, corresponding to an overall capacity of ~210mAh/g. Further cycling of the cell between 4.5 and 2 V shows a voltage profile that becomes increasing spinel-like in character, particularly during discharge, with capacity increasing at 4 V at the expense of capacity at 3 V (Fig. 49b). Although detailed information of the structural changes that occur during the initial extraction of lithium from orthorhombic-$LiMnO_2$ is not yet available, it would appear from the X-ray diffraction

patterns obtained from delithiated electrodes during the first charge that delithiation is accompanied almost immediately by an onset of the transition to the spinel structure (Fig. 50(a-d)) [167]. It is clear, however, that several cycles are required to complete the phase transition; the powder X-ray diffraction pattern of an electrode after 10 cycles, obtained when the overall composition of the electrode was $Li_{0.4}MnO_2$ is representative of a single-phase spinel structure (Fig. 50e). Surprisingly, some of these electrochemically-generated spinel electrodes show significantly better capacity retention than standard $Li[Mn_2]O_4$ spinel electrodes when cycled over both the 4 and 3 V regions. For example, a sample prepared under argon from the reaction of γ-MnO_2 with LiOH in the presence of some carbon, shows extremely stable cycling behavior over both the 3 V and 4 V plateaus with a rechargeable capacity of 120 mAh/g (Fig. 49c) [167]; the reasons for this good behavior from an electrode with spinel-type character are not yet understood. These findings have been confirmed in several independent studies of the orthorhombic-$LiMnO_2$ system [171-174].

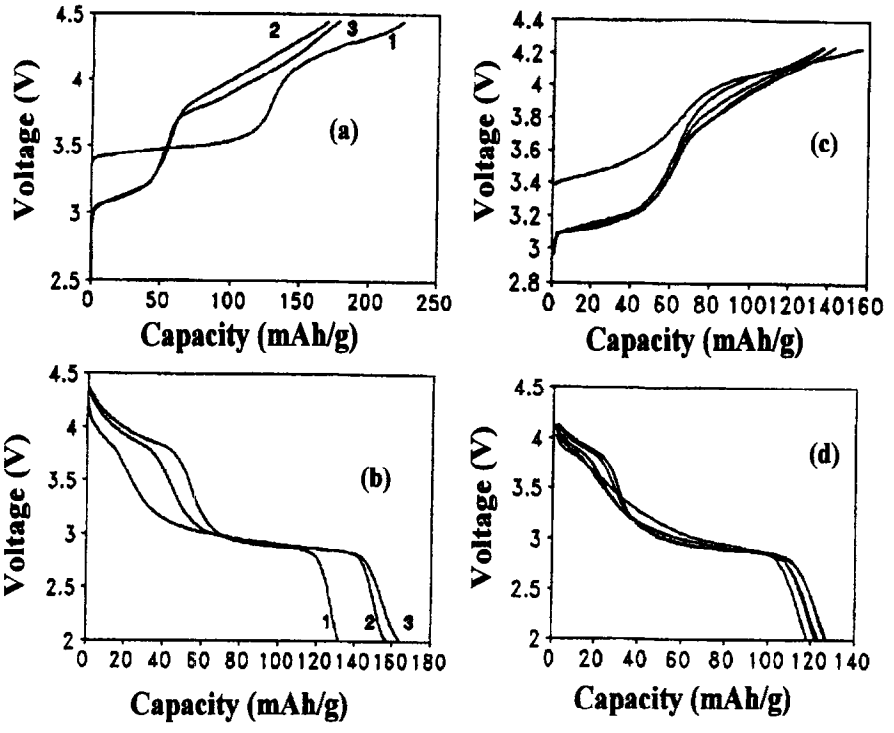

Fig. 49.

Charge and discharge profiles of Li/orthorhombic-$LiMnO_2$ cells (0.1 mA/cm^2) : (a) and (b) 2.50 - 4.45 (V); (c) and (d) 2.50 - 4.25 V. ($LiMnO_2$ prepared at 600°C, 4h) [167].

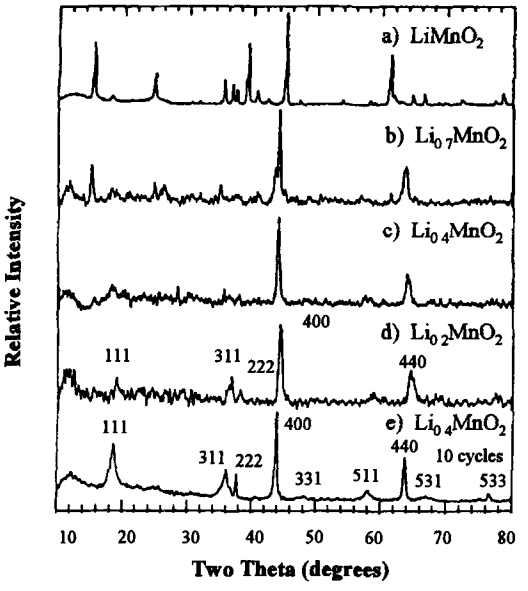

Fig. 50.

Powder X-ray diffraction patterns of Li_xMnO_2 from orthorhombic-$LiMnO_2$; (a) x = 1.0, (b) x = 0.7, (c) x = 0.4, (d) x = 0.2 and (e) x ≈ 0.4 after 10 cycles [167].

A possible mechanism for the transformation of the orthorhombic-$LiMnO_2$ structure to a $Li_x[Mn_2]O_4$ spinel has been proposed [167]. Two parallel slices that alternate through the orthorhombic $LiMnO_2$ structure are shown in Fig. 51(a and b); corresponding slices of the spinel structure are shown in Fig. 51(c and d), respectively. Shaded octahedra represent manganese-occupied octahedra; clear octahedra represent either lithium-occupied or vacant octahedra. On lithium extraction from orthorhombic-$LiMnO_2$, the displacement of one manganese ion into a neighboring vacant octahedral site (curved arrow) causes the displacement of one other manganese ion (straight arrow). This transformation requires a displacement of 50% of the manganese ions to generate the 3:1 ratio of manganese ions in alternate layers between layers of cubic-close-packed oxygen planes which is required by the ideal $Li[Mn_2]O_4$ structure. Like many other lithiated manganese oxides, the electrochemical behavior of orthorhombic-$LiMnO_2$ emphasizes the stability of the spinel structure to lithium insertion and extraction, and its utility as a host electrode for rechargeable lithium cells.

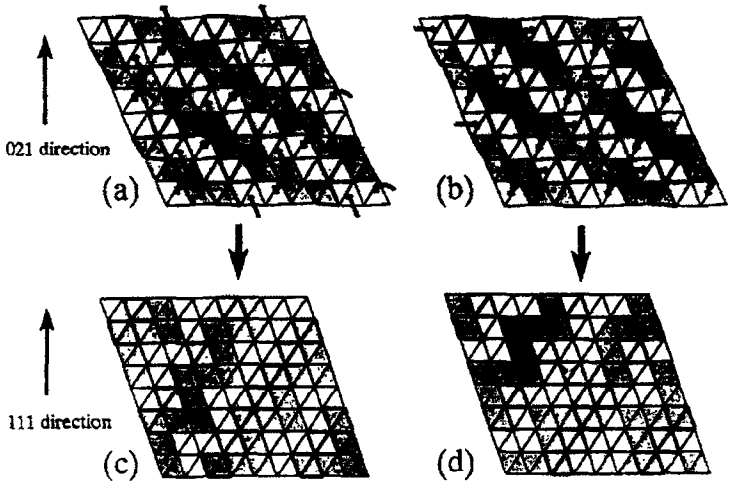

Fig. 51.

A proposed mechanism for the movement of manganese ions during the transformation of orthorhombic-$LiMnO_2$ to the spinel structure [167].

3.8 Cation-stabilized MnO_2 Electrodes

This review has highlighted the stability of spinel-type structures and, in particular, the stability of the $[Mn_{2-x}Li_x]O_4$ spinel framework and the tendency for many lithiated manganese oxide electrodes to transform to the spinel structure during cycling. Unfortunately, however, the Jahn-Teller effect which arises in close-packed lithium-manganese-oxide spinels when the average manganese oxidation state falls below 3.5 results in structural distortions in the electrodes that damage the structural integrity of the electrode and cause capacity loss effects. One approach that has been adopted in an attempt to prevent the conversion to spinel has been to investigate the possible use of non-close-packed manganese oxide structures that are stabilized by cations larger than lithium.

3.8.1 $Na_{0.44}MnO_2$. $Na_{0.44}MnO_2$ is prepared by reacting a sodium compound such as Na_2CO_3 or $NaNO_3$ with a manganese compound such as $MnCO_3$ or $Mn(NO_3)_2$ in the required stoichiometric ratio in air at 800°C [175]. Rietveld analysis of $Na_{0.44}MnO_2$ shows that it is isostructural with $Na_4Mn_4Ti_5O_{18}$ [176]. The structure of $Na_{0.44}MnO_2$ proposed by Doeff et al is shown in Fig. 52 [175]. The packing of the oxygen array is irregular because of localized regions in the structure that contain the large Na^+ ions, thus providing an interstitial space in the MnO_2 framework of unusual dimensions. The structure contains of columns of edge-sharing square pyramids and sheets of edge-sharing octahedra two and three units in width that run parallel to the *c*-axis of the unit cell. The structure has two types of tunnel, one large S-shaped

tunnel, and two identical pentagonally shaped tunnels. The pentagonal tunnels are almost fully occupied, whereas the four sodium sites in the S-shaped tunnels are partially occupied. The sodium ions can be partially ion-exchanged with lithium either prior to use or *in-situ* during electrochemical discharge and charge. Despite the ability to ion-exchange with lithium, $Na_{0.44}MnO_2$ electrodes have been reported to be resistant to a transformation to a spinel-type structure, suggesting that not all the sodium ions can be readily removed from the structure. Lithium-exchanged $Na_{0.14}Li_{0.3}MnO_2$ electrodes have been evaluated in lithium-polymer electrochemical cells at 85°C. Preliminary data have shown that these electrodes can deliver approximately 140mAh/g when discharged between 3.77 and 1.8 V at 0.115 mA/cm^2 (Fig. 53) [175]. Complete recovery of the capacity is obtained if cells are charged at a slow rate (0.05 mA/cm^2).

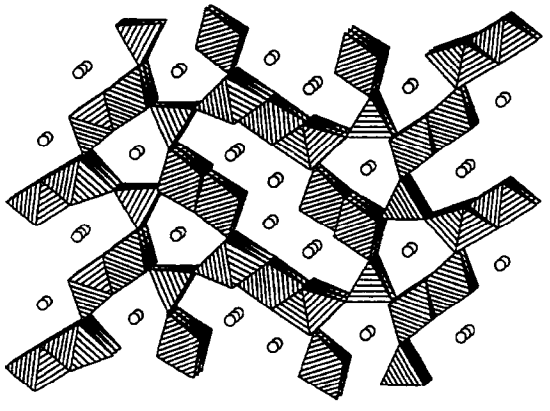

Fig. 52.

The structure of orthorhombic-$Na_{0.44}MnO_2$ proposed by Doeff et al [175].

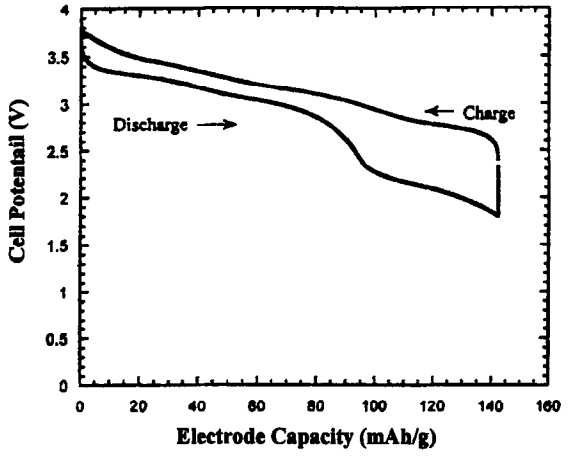

Fig. 53.

The discharge and charge voltage profiles during the first cycle of a Li/PEO_6•LiTFSI/$Na_{0.14}Li_xMnO_2$ cell operated at 85°C, where PEO_8•LiTFSI refers to the polyethylene oxide polymer electrolyte with a lithium trifluoromethane-sulfonylimide salt [175].

3.8.2 Romanechite-MnO_2 and Todorokite-MnO_2 Structures. Several MnO_2 framework structures with strings of edge-sharing MnO_6 octahedra and large tunnels exist in nature. The tunnels contain water and stabilizing cations which prevent the tunnels from collapsing. For example, hollandite-type structures, (Ba, K) $_{1-2}Mn_8O_{16}\cdot xH_2O$, have tunnels of relative dimension (2 x 2) (see section 3.3.1), romanechite-type structures, (Ba, K, Mn^{2+}, $Co)_2Mn_5O_{10}\cdot xH_2O$ have tunnels of size (2 x 3) [177] and todorokite-type structures, (Ca, Na, K)(Mg, Mn^{2+})Mn_5O_{12} have tunnels of size (3 x 3) [178-179], as shown in Figs. 54 (a-c). The tunnels are occupied by stabilizing cations and water molecules. High resolution transmission electron microscopy studies have shown that these tunnel structures, for example, hollandite and romanechite, can exist as intergrowths in a coherent manner on the unit cell level without any apparent ordering of the structure types [177-179].

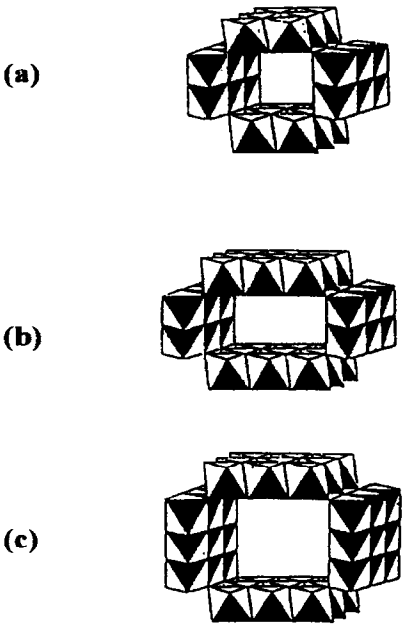

Fig. 54.

The MnO_2 framework structures of (a) hollandite-MnO_2, (b) romanechite-MnO_2 and (c) todorokite-MnO_2. The large tunnels contain water and stabilizing cations such Ba^{2+}, Mg^{2+}, Mn^{2+}, K^+, and Na^+ (not shown) [10].

Although these materials are not expected to provide commercially attractive electrode materials for lithium battery applications, preliminary data have shown that they have interesting electrochemical properties [180]. For example, a typical cycling profile for a Mg-stabilized todorokite electrode is shown in Fig. 55 [180]. The electrodes provide a capacity corresponding to 0.56 Li per Mn; the cell operates with 100% coulombic efficiency at a very low current rate (20 $\mu A/cm^2$).

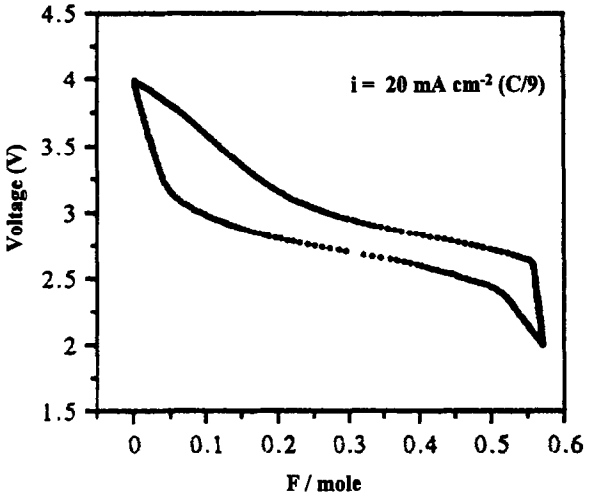

Fig. 55.

A typical electrochemical discharge and charge profile obtained from a lithium cell containing a Mg-stabilized todorokite-MnO_2 positive electrode [180].

CONCLUDING REMARKS

This review has highlighted the structural versatility of the lithium-manganese-oxide system, but also the limitations of the various structure types when used as insertion electrodes in rechargeable lithium batteries. The structural stability of these compounds to lithium insertion/extraction reactions is compromised by several factors: 1) an instability of the oxygen array, which can shear from hexagonal close packing to cubic-close packing with a significant increase or decrease in the unit cell parameters and volume, 2) mobility of manganese ions within the host structure, 3) reactivity of extensively delithiated compounds (which become highly oxidizing when the composition approaches MnO_2) toward the organic electrolytes, 4) solubility of the electrode in the electrolyte, and 5) crystallographic (Jahn-Teller) anisotropic distortions that take place when the Mn^{3+}-ion concentration reaches a critical value. There is a strong tendency for many lithium manganese oxides to transform to a spinel-type structure, either during electrochemical cycling or by heat-treatment; these findings emphasize the stability of the $[Mn_{2-x}Li_x]O_4$ spinel framework as a host structure for lithium. Spinel electrodes, such as the 4 V system $Li_{1.05-x}Mn_{1.95}O_4$ ($0 \leq x \leq 0.85$), and the 3 V system $Li_{4+x}Mn_5O_{12}$ ($0 \leq x \leq 6.5$) that maintain cubic symmetry during cycling, have shown promise as viable electrode materials. Unfortunately, these materials are limited by their relative low capacities (100-150 mAh/g) compared to layered $LiCo_{1-x}Ni_xO_2$ structures that offer significantly higher capacities (150 - 200 mAh/g) at 3.5 - 4.0 V. "CDMO" (3 V) electrodes which consist of a lithiated γ-MnO_2 structure stabilized by domains of spinel provide slightly superior capacities than $Li_4Mn_5O_{12}$ spinel electrodes. However, CDMO materials are not attractive electrodes for lithium-ion cells

(which are conveniently assembled in the discharged state) because of their relatively low voltage vs. lithium and the fact that it is difficult to fabricate them in a fully lithiated (discharged) condition. Strong challenges, therefore, remain that will require innovative approaches to fabricate new structures or to stabilize existing ones to strengthen the possibility of using lithium manganese oxide electrodes on a large scale in rechargeable lithium batteries.

REFERENCES

1. K. Kordesch, L. Binder, W. Taucher, Ch. Faistauer and J. Daniel-Ivad, *Power Sources 14*, (Eds. A. Attwell and T. Kelly), Proc. 18th Int. Power Sources Symp. (1993).
2. Y. Chabre and J. Pannetier, *Prog. in Solid State Chem.*, **23**, 1 (1995).
3. Y. Idota, M. Mishima, Y. Miyaki, T. Kubota and T. Miyasaka, Fuji Photo Film Co., Ltd, Canadian Patent Application, 2,134,052 (1995).
4. M. M. Thackeray, M.H. Rossouw, A. de Kock, A.P. de la Harpe, R.J. Gummow, K. Pearce and D.C.Liles, *J. Power Sources*, **43-44**, 289 (1993).
5. M.S. Whittingham, *Prog. Solid State Chem.*, **12**, 41 (1978).
6. T.A. Hewston and B.L. Chamberland, *J.Phys. Chem. Solids*, **48**, 97 (1987).
7. D.W. Murphy, *Advances in the Synthesis and Reactivity of Solids*, **1**, 237 (1991).
8. *Lithium Batteries, New Materials, Developments and Perspectives* (Ed.: G. Pistoia), Industrial Chemistry Library, Volume 5, Elsevier, Amsterdam (1994).
9. S. Megahed and B. Scrosati, *J. Power Sources*, **51**, 79 (1994).
10. M.M. Thackeray, *Prog. in Batt. and Batt. Mat.*, **14**, 1 (1995).
11. M.M. Thackeray, *J. Electrochem. Soc.*, **142**, 2558 (1995).
12. R. Koksbang, J. Barker, H. Shi and M.Y. Saidi, *Solid State Ionics*, **84**, 1 (1996).
13.** M.M. Thackeray, in *Handbook of Battery Materials*, (Ed.: J.O. Besenhard), VCH Verlagsgesellschaft mbH. (1997). In press.
14. T. Ohzuku and M. Kitagawa, T. Hirai, *J. Electrochem. Soc.*, **137**, 40 (1990).
15. M.M. Thackeray, W.I.F. David and J.B. Goodenough, *Mat. Res. Bull.*, **17**, 785 (1982).
16. M.M. Thackeray, W.I.F. David, P.G. Bruce and J.B. Goodenough, *Mat. Res. Bull.*, **18**, 461 (1983).
17. J.B. Goodenough, M.M. Thackeray, W.I.F. David and P.G. Bruce, *Rev. de Chim Min.*, **21**, 435 (1984).

18. M.M. Thackeray, P.J. Johnson, L.A. de Picciotto, P.G. Bruce and J.B. Goodenough, *Mat. Res. Bull.*, **19**, 179 (1984).

19. M.M. Thackeray and J.B. Goodenough, U.S. Patent 4,507,371 (1985).

20. T. Ohzuku, M. Kitagawa and T. Hirai, *J. Electrochem. Soc.*, **137**, 769 (1990).

21. J.M. Tarascon, E. Wang, F.K. Shokoohi, W.R. McKinnon and S. Colson, *J. Electrochem. Soc.*, **138**, 2859 (1991).

22. J.M. Tarascon and D. Guyomard, *J. Electrochem. Soc.*, **138**, 2864 (1991).

23. M.M. Thackeray, A. de Kock, M.H. Rossouw, D.C. Liles, R. Bittihn and D. Hoge, *J. Electrochem. Soc.*, **139**, 364 (1992).

24. D. Guyomard and J.M. Tarascon, *J. Electrochem. Soc.*, **139**, 937 (1992).

25. R.J Gummow, A. De Kock and M.M. Thackeray, *Solid State Ionics*, **69**, 59 (1994).

26. J.M. Tarascon, W.R. McKinnon, F. Coowar, T.N. Bowmer, G. Amatucci and D. Guyomard, *J. Electrochem. Soc.*, **141**, 1421 (1994).

27. D. Guyomard and J.M. Tarascon, *Solid State Ionics*, **69**, 222 (1994).

28. D.W. Murphy, R.J. Cava, S.M. Zahurak and A. Santoro, *Solid State Ionics*, **9-10**, 413 (1983).

29. K.M. Colbow, J.R. Dahn and R.R. Haering, J. Power Sources, **26**, 397 (1989).

30. E. Ferg, R.J. Gummow, A. de Kock and M.M. Thackeray, *J. Electrochem. Soc.*, **141**, L147 (1994).

31. T. Ohzuku, A. Ueda and N. Yamamoto, J. Electrochem. Soc., **142,** 1431 (1995).

32. R.J. Gummow, M.M. Thackeray and W.I.F. David, S.Hull, *Mat. Res. Bull.*, **27**, 327 1992).

33. E. Rossen, J.N. Reimers and J.R. Dahn, *Solid State Ionics*, **62,** 53 (1993).

34. R.J. Gummow and M.M. Thackeray, *J. Electrochem. Soc.*, **140**, 3365 (1993).

35. L.A. de Picciotto and M.M. Thackeray, *Solid State Ionics*, **18-19**, 773 (1986).

36. L.A. de Picciotto, M.M. Thackeray and G. Pistoia, *Solid State Ionics*, **28-30**, 1364 (1988).

37. G. Pistoia, M. Pasquali, L.A. de Picciotto and M.M. Thackeray, *Solid State Ionics*, **28**, 879 (1988).

38. L. Guohua, S. Sakuma, H. Ikuta, T. Uchida, M. Wakihara and G. Hetong, *Denki Kagaku*, **64**, 202 (1996).

39. C. Masquelier, M. Tabuchi, K. Ado, R. Kanno, Y.Kobayashi, Y. Maki, O. Nakamura and J.B. Goodenough, *J. Solid State Chem.*, **123**, 255 (1996).

40. P. Strobel, F. Le Cras and M. Anne, *J. Solid State Chem.*, **124**, 83 (1996).

41. D.G. Wickham and W.J. Croft, *J. Phys. Chem. Solids*, **7**, 351 (1958).

42. K. Miura, A. Yamada and M. Tanaka, *Electrochimica Acta*, **41**, 249 (1996).

43. G. Pistoia, G. Wang and C. Wang, *Solid State Ionics*, **58**, 285 (1992).

44. G. Pistoia and G. Wang, *Solid State Ionics*, **66**, 135 (1993).

45. G. Pistoia, D. Zane and Y. Zhang, *J. Electrochem. Soc.*, **142**, 2551 (1995).

46. Y. Xia, H. Takeshige, H. Noguchi and M. Yoshio, *J Power Sources*, **56**, 61 (1995).

47. Y. Xia, H. Noguchi and M. Yoshio, *J Solid State Chem.*, **119**, 216 (1995).

48. V. Manev, A. Momchilov, A. Nassalevska and A. Sato, *J Power Sources*, **54**, 323 (1995).

49. J. Barker, R. Pynenburg and R. Koksbang, *J. Power Sources*, **52**, 185 (1994).

50. Y. Saidi, J. Barker and R. Koksbang, *J. Solid State Chem.*, **122**, 195 (1996).

51. R. Koksbang, J. Barker, M.Y. Saidi, K. West, B. Zachau-Christiansen and S. Skaarup, *Solid State Ionics*, **83**, 151 (1996).

52. M.Y. Saidi, J. Barker and R. Koksbang, *Electrochim Acta*, **41**, 199 (1996).

53. L. Feng, Y. Chang and T. Lu, *J. Power Sources*, **63**, 149 (1996).

54. W.I.F. David, M.M. Thackeray, L.A de Picciotto and J.B. Goodenough, *J. Solid State Chem.*, **67**, 316 (1987).

55. J.C. Hunter, J. Solid State Chem., **39**, 142 (1981).

56. A. Mosbah, A. Verbaere and M. Tournoux, *Mat. Res. Bull.*, **18**, 1375 (1983).

57. A. Yamada and M. Tanaka, Mat. Res. Bull., **30**, 715 (1995).

58. A. Yamada, *J. Solid State Chem.*, **122**, 160 (1996).

59. W.I.F. David, J.B. Goodenough, M.M. Thackeray and M.G.S.R. Thomas, *Rev. de Chim. Minér.*, **20**, 636 (1983).

60. A. de Kock and M.M. Thackeray. Unpublished results.

61. D.H. Yang, Y.J. Shin and S.M. Oh, *J. Electrochem. Soc.*, **143**, 2204 (1996).

62. M.M. Thackeray and R.J. Gummow, US Patent 5,316,872.

63. T. Takada, H. Hayakawa and E. Akiba, *J. Solid State Chem.*, **115**, 420 (1995).

64 R. Bittihn, R. Herr and D. Hoge, *J. Power Sources*, **43-44**, 223 (1993).

65. L. Guohua, H. Ikuta, T. Uchida and W. Wakihara, *J. Electrochem. Soc.*, **143**, 178 (1996).

66. K. Amine, H. Tukamoto, H. Yasuda and Y. Fujita, *J. Electrochem. Soc.*, **143**, 1607 (1996).

67. Y. Gao, K. Myrtle, M. Zhang, J.N. Reimers and J.R. Dahn, *Phys. Rev.*, **54 (24)**, 1 (1996).

68. Q. Zhong, A. Bonakdarpour, M. Zhang, Y. Gao and J.R. Dahn, *J. Electrochem. Soc.*, **144**, 205 (1997).

69. C. Sigala, D. Guyomard, A. Verbaere, Y. Piffard and M. Tournoux, *Solid State Ionics*, **81**, 167 (1995).

70. A.D. Robertson, W.F. Howard, S.H. Lu and W.F. Averill, *Ext. Abstr.*, 190th Meeting of the Electrochemical Society, San Antonio (6-11 October), p. 1010 (1996).

71. A. de Kock, M.H. Rossouw, L.A. de Picciotto, M.M. Thackeray, W.I.F.David and S.Hull, *Mat. Res. Bull.*, **25**, 657 (1990).

72. M.M. Thackeray and A. de Kock, *Mat. Res. Bull.*, **28**, 1041 (1993)

73. M. Jansen and R. Hoppe, *Allg. Chem.*, **397**, 279 (1973).

74. P. Barboux, J.M. Tarascon and F.K. Shokoohi, *J. Solid State Chem.*, **94** 185 (1991).

75. A. Momchilov, V. Manev, A. Nassalevska and A. Kozawa, *J. Power Sources*, **41**, 305 (1993).

76. M.N. Richard, E.W. Fuller and J.R. Dahn, *Solid State Ionics*, **73**, 81 (1994).

77. V. Manev, B. Banov, A. Momchilov and A. Nassalevska, *J. Power Sources*, **57**, 99 (1995).

78. Y. Xia and M. Yoshio, *J. Power Sources*, **57**, 125 (1995).

79. A. Yamada, K. Miura, K. Hinokuma and M. Tanaka, *J. Electrochem. Soc.*, **142**, 2149 (1995).

80. Y. Gao and J.R. Dahn, *Solid State Ionics*, **84**, 33 (1996).

81. M.M. Thackeray, M.F. Mansuetto, D.W. Dees and D.R.Vissers, *Mat. Res. Bull.*, **31**, 133 (1996).

82. M.M. Thackeray, M.F. Mansuetto and C.S. Johnson, *J. Solid State Chem.*, **125**, 274 (1996).

83. Y. Gao and J.R. Dahn, *J. Electrochem. Soc.*, **143,** 100 (1996).

84. Y. Xia and M. Yoshio, *J. Electrochem. Soc.*, **143**, 825 (1996).

85. W. Liu, G.C. Farrington, F. Chaput and B. Dunn, *J. Electrochem. Soc.*, **143**, 879 (1996).

86. Z. Jiang and K.M. Abraham, *J. Electrochem. Soc.*, **143**, 1591 (1996).

87. Y. Gao and J.R. Dahn, *J. Electrochem. Soc.*, **143,** 1783 (1996).

88. W. Liu, K. Kowal and G.C. Farrington, *J. Electrochem. Soc.*, **143**, 3590 (1996).

89. P. Endres, B. Fuchs, S. Kemmler-Sack, K. Brandt, G. Faust-Becker and H.-W. Praas, *Solid State Ionics*, **89**, 221 (1996).

90. C. Tsang and A. Manthiram, *Solid State Ionics*, **89**, 305 (1996).

91. D. Larcher, B. Gerand and J.-M. Tarascon, *Ext. Abstr.*, 190th Meeting of the Electrochemical Society, San Antonio (6-11 October), p. 1012 (1996).

92. M. Keller and R. Dieckmann, *Ber. Bunsenges. Phys. Chem.*, **89**, 1095 (1985).

93. H. Ikuta, M. Hosoya, K. Koga, T. Uchida and M. Wakihara, *Ext. Abstr. II-B-48*, 8th Int. Meeting on Lithium Batteries, Nagoya, Japan, (June 16-21, 1996).

94. J.B. Bates, D. Lubben, N.J. Dudney and F.X. Hart, *J. Electrochem. Soc.*, **142,** L149 (1995).

95. J.B. Bates, D. Lubben, N.J. Dudney, R.A. Zuhr and F.X. Hart, *Proc. Symp. Electrochem Soc.*, **95-22**, 215 (1995).

96. X. Yu, J. B. Bates, G.E. Jellison and F. X. Hart, *J. Electrochem. Soc.*, **144**, 524 (1997).

97.** M.M. Thackeray, M.F. Mansuetto and J.B. Bates, *J. Power Sources*, (1996). In press.

98.** M.M. Thackeray, *J. Electrochem. Soc.*, (1997). In press.

99. C. Delmas, S. Bréthes and M. Ménétrier, *J. Power Sources*, **34**, 113 (1991).

100. C. Delmas, in reference 8, 457.

101 F.K. Shokoohi, J.M. Tarascon, B.J. Wilkens, D. Guyomard and C.C. Chang, *J Electrochem. Soc.*, **139**, 1845 (1992).

102. K.-H. Hwang, S.-H. Lee and S.-K Joo, *J. Electrochem. Soc.*, **141**, 3296 (1994).

103. K.A. Striebel, C.Z. Deng, S.J. Wen and E.J. Cairns, *J. Electrochem. Soc.*, **143**, 1821 (1996).

104. T. Ohzuku, M. Kitagawa, K. Sawai and T. Hirai, *J. Electrochem. Soc.*, **138**, 360 (1991)

105. M.H. Rossouw, D.C. Liles, M.M. Thackeray, W.I.F. David and S. Hull, *Mat. Res. Bull.*, **27**, 221 (1992).

106. M.H. Rossouw, D.C. Liles and M.M. Thackeray, *Prog. in Batt. and Batt Mat.*, **15**, 8 (1995).

107** C.S. Johnson, D.W. Dees, M.F. Mansuetto, M.M. Thackeray, D.R. Vissers, D. Argyriou, C.-K. Loong and L. Christensen, *J. Power Sources*, (1997). In press.

108. M.A. Humbert, Ph. Biensan, M. Broussely, A. Lecerf, A. Dollé and H. Ladhily, *J. Power Sources*, **43-44**, 681 (1993).

109 Ph. Botkowitz, Ph. Deniard, M. Tournoux and R. Brec, *J. Power Sources*, **43-44**, 657 (1993).

110. Ph. Botkowitz, R. Brec, Ph. Deniard, M. Tournoux and G.Burr, *Mol. Cryst. Liq. Cryst.*, **244**, 233 (1994).

111. C.S. Johnson and M.M. Thackeray. Unpublished results.

112.** C.S. Johnson, M.F. Mansuetto, M.M. Thackeray, Y. Shao-Horn and S.A. Hackney, J. Electrochem. Soc., (1997). In press.

113. W.I.F. David, M.M. Thackeray, P.G. Bruce and J.B. Goodenough, *Mat. Res. Bull.*, **19**, 99 1984).

114. W.I.F. David, P.G. Bruce and J.B. Goodenough, *J. Solid State Chem.*, **50**, 235 (1983).

115 D.W. Murphy, F.J. Di Salvo, J.N. Carides and J.V. Waszczak, *Mat. Res. Bull.*, **13,** 1395 (1978).

116 M.M. Thackeray, A. de Kock, L.A. de Picciotto and G. Pistoia, *J. Power Sources*, **26**, 355 (1989).

117. J.B. Fernandes, D. Desai, V.N. Kamat Dalal, *J. Power Sources*, **15**, 209 (1985).

118.** H. Ikeda and S. Narukawa, *J. Power Sources*, **9**, 329 (1983).

119. T. Ohzuku, M. Kitagawa and T. Hirai, *J. Electrochem. Soc.*, **136**, 3169 (1989).

120. M.M. Thackeray, M.H. Rossouw, R.J. Gummow, D.C. Liles, K. Pearce, A. de Kock, W.I.F. David and S. Hull, *Electrochim. Acta*, **38**, 1259 (1993).

121. T. Nohma, T. Saito, N. Furukawa and H. Ikeda, *J. Power Sources*, **26**, 389 (1989).

122. T. Nohma, Y. Yamamoto, K. Nishio, I. Nakane and N. Furukawa, *J. Power Sources*, **32**, 373 (1990).

123. M. Yoshio, S. Inoue, G. Piao and H. Nakamura, *Prog. in Batteries and Solar Cells*, **9**, 205 (1990).

124. M. Yoshio, S. Inoue, M. Hyatutake, G. Piao and H. Nakamura, *J. Power Sources*, **34**, 147 (1991).

125. M. Yoshio, H. Nakamura and H. Noguchi, *Prog. in Batteries and Battery Materials*, **10**, 171 (1991).

126. L. Li and G. Pistoia, *Solid Sate Ionics*, **47**, 231 (1991).

127. L. Li and G. Pistoia, *Solid Sate Ionics*, **47**, 241 (1991).

128. T. Nohma, Y. Yamamoto, I. Nakane and N. Furukawa, *J. Power Sources*, **39**, 51 (1992).

129. H. Watanabe, T. Nohma, I. Nakane, S. Yoshimura, K. Nishio and T. Saito, *J. Power Sources*, **43-44**, 217 (1993).

130. T. Nohma, A. Yanai, S. Yoshimura, K. Nishio, Y. Yamamoto, S. Fukuoka and M. Hara, *Ext. Abstr. II-B-45*, 8th Int. Meeting on Lithium Batteries, Nagoya, Japan, (June 16-21, 1996).

131. Y. Shao and S. Hackney, *Ext. Abstr.*, 189th Meeting of the Electrochemical Society, Los Angeles (5-10 May), p. 58 (1996).

132. K. Mizushima, P.C. Jones, P.J. Wiseman and J.B. Goodenough, *Mat. Res. Bull.*, **15**, 783 (1980).

133 J.N. Reimers and J.R. Dahn, *J. Electrochem. Soc.*, **139**, 2091 (1992).

134. T. Ohzuku, A. Ueda, N. Nagayama, Y Iwakoshi, and H. Komori, *Electrochim. Acta*, **38**, 1159 (1993).

135 T. Ohzuku, A. Ueda and M. Nagayama, *J. Electrochem. Soc.*, **140**, 1862 (1993)

136. H. Arai, S. Okada, H.Ohtsuka, M. Ichimura and J. Yamaki, *Solid State Ionics*, **80**, 261 (1995).

137. T. Ohzuku, A. Ueda and M. Kouguchi, *J. Electrochem. Soc.*, **142**, 4033 (1995).

138. A. Rougier, P. Gravereau and C. Delmas, *J. Electrochem. Soc.*, **143**, 1168 (1996).

139.** W. Li and J.C. Currie , *J. Electrochem. Soc.*, (1997). Submitted for publication.

140. T. Ohzuku and A. Ueda, *J. Electrochem. Soc.*, **141**, 2972 (1994).

141. T. Ohzuku, H. Fukuda and T. Hirai, *Chemistry Express*, **2**, 543 (1987).

142. P. Strobel, *Solid State Ionics III*, MRS Symp. Proc. **293**, 63 (1993).

143. P. Strobel and C. Mouget, *Mat. Res. Bull.*, **28**, 93 (1993).

144. P. Strobel and J. C. Charenton, *Rev. de Chim. Miner.*, **23**, 125 (1986).

145. P. Strobel, J. C. Charenton and M. Lenglet, *Rev. de Chim. Miner.*, **24**, 199 (1987).

146. M. Tsuji, S. Komarneni, Y. Tamaura and M. Abe, *Mat. Res. Bull.*, **27**, 741 (1992).

147. F. Leroux, D. Guyomard and Y. Piffard, *Solid State Ionics*, **80**, 299 (1995).

148. F. le Roux, D. Guyomard and Y. Piffard, *Solid State Ionics*, **80**, 307 (1995).

149. S. Bach, J.P. Pereira-Ramos and N. Baffier, *J. Electrochem. Soc.*, **143**, 3429 (1996).

150. R. Chen, P. Zavalij and M.S. Whittingham, *Chem. Mater.*, **8**, 1275 (1996).

151. F. le Cras, S. Rohs, M. Anne and P.Strobel, *J. Power Sources*, **54**, 319 (1995).

152. P. Strobel, F. Le Cras, S. Rohs and L. Pontonnier, *Mat. Res. Bull.*, **31**, 1417 (1996).

153. M.H. Rossouw and M.M. Thackeray, *Mat. Res. Bull.*, **26**, 463 (1991).

154. F. Lubin, A. Lecerf, M. Broussely and J. Labat, *J. Power Sources*, **34**, 161 (1993).

155. F. Lubin, PhD Thesis, Institut National des Sciences Appliquées de Rennes, France, (1991).

156. M.H. Rossouw, D.C. Liles and M.M. Thackeray, *J. Solid State Chem.*, **104**, 464 (1995).

157. B. Fuchs and S. Kemmler-Sack, *Solid State Ionics*, **68**, 279 (1994).

158. A.R. Armstrong and P.G. Bruce, *Nature*, **381**, 499 (1996).

159. C. Delmas and F. Capitaine, *Ext. Abstr. II-B-33*, 8th Int. Meeting on Lithium Batteries, Nagoya, Japan, (June 16-21, 1996).

160. F. Capitaine, P. Gravereau and C. Delmas, *Solid State Ionics*, **89**, 197 (1996).

161. J.N. Reimers, W. Li, E. Rossen and J.R. Dahn, *Mater. Res. Soc. Symp. Proc.*, **293**, 3 (1993).

162. Y. Shao-Horn, S.A. Hackney, R. Gitzendanner, P.G. Bruce, C.S. Johnson and M.M. Thackeray, *Ext. Abstr.*, 192nd Meeting of the Electrochemical Society, Paris (October, 1997).

163. L.A. de Picciotto, M.M. Thackeray, W.I.F. David, P.G. Bruce and J.B. Goodenough, *Mat. Res. Bull.*, **19**, 1497 (1984).

164. L.A. de Picciotto, M.M. Thackeray, W.I.F. David, P.G. Bruce and J.B. Goodenough, *J. Solid State Chemistry*, **67**, 285 (1987).

165. R. Hoppe, G. Brachtel and M. Jansen, *Z. Anorg. Allg. Chem.*, **417**, 1 (1975).

166. I.J. Davidson, R.S. McMillan, J.J. Murray and J.E. Greedan, *J. Power Sources*, **54**, 232 (1995).

167. R.J. Gummow, D.C. Liles and M.M. Thackeray, *Mat. Res. Bull.*, **28**, 1249 (1993).

168. T. Ohzuku, A. Ueda and T. Hirai, *Chemistry Express*, **7**, 193 (1992).

169. J.N. Reimers, E.W. Fuller, E. Rossen and J.R. Dahn, *J. Electrochem. Soc.*, **140**, 3396 (1993).

170. I. Koetschau, M.N. Richard, J.R. Dahn, J.B. Soupart and J.C. Rousche, *J. Electrochem. Soc.*, **142**, 2906 (1995).

171. R.J. Gummow and M.M. Thackeray, *J. Electrochem. Soc.*, **141**, 1178 (1994).

172. M Tabuchi, K. Ado, C. Masquelier, I. Matsubara, H. Sakaebe, H. Kageyama, H. Kobayashi, R. Kanno and O.Nakamura, *Solid State Ionics*, **89**, 53 (1996).

173. L. Croguennec, P. Deniard, R. Brec, P. Biensan and M. Broussely, *Solid State Ionics*, **89**, 127 (1996).

174. T. Ohzuku, S. Kitano, M. Iwanaga, H. Matsumo and A. Ueda, *J. Power Sources*, (1997). In press.

175. M.M. Doeff, T.J. Richardson, L. Kepley, *J. Electrochem. Soc.*, **143**, 2507 (1996).

176. W.G. Mumme, *Acta Cryst.*, **B24**, 1114 (1968).

177. S. Turner and P.R. Buseck, *Science*, **203**, 456 (1979).

178. S. Turner and P.R. Buseck, *Science*, **212**, 1024 (1981).

179. S. Turner, M.D. Siegel and P.R. Buseck, *Nature*, **296**, 841 (1982).

180. M.J. Duncan, F. Leroux and L.F. Nazar, *Ext. Abstr. No. 817*, 190th Meeting of the Electrochemical Society, San Antonio (6-11 October), p. 1001 (1996).